December 2016

Optimal Operation of a Northwest Grid of Saudi Arabia Including Renewable Resources

Hani Albalawi
Clemson University, halbala@clemson.edu

OPTIMAL OPERATION OF A NORTHWEST GRID OF SAUDI ARABIA INCLUDING RENEWABLE RESOURCES

A Dissertation
Presented to
the Graduate School of
Clemson University

In Partial Fulfillment
of the Requirements for the Degree
Doctor of Philosophy
Electrical Engineering

By
Hani Albalawi
December 2016

Accepted by:
Dr. Elham Makram, Committee Chair
Dr. Richard Groff
Dr. Anthony Martin
Dr. William Bridges

ABSTRACT

The use of fossil fuel, which has been one of the major sources of energy of the modern world, has led to environmental concerns. One solution to these issues is the application of renewable energy, which can also address the fluctuation in fuel prices. The Kingdom of Saudi Arabia (KSA) faces a demand of energy expected to exceed 120 GW by 2032.

The government is taking appropriate actions, introducing sustainable renewable energy not only to meet the demand with clean energy sources but also to reduce the Kingdom's consumption of fuel and gas. KSA, which has a high irradiation rate especially in the northwest area, Tabuk Region, plans to invest 41 GW maximum of solar power. In light of this decision, this research will present a comprehensive study of PV penetration up to peak output of 40 MW with battery storage to the isolated northwest grid, Tabuk Grid, as a first stage development.

However, the increase of grid-connected photovoltaic (PV) in the presence of nonlinear loads, and the growth of power electronic applications produce harmonics in the power system. These harmonics may distort the current and voltage waveforms which impact the power quality and affect the operation of all electric devices.

Renewable energy systems nowadays are sufficiently developed to be widely used for environmental and economic dispatch (ED) concerns. However, renewable energy that are not geographically distributed present a considerable challenge with respect to variability and availability. One of the solutions for addressing the challenge of solar variability is to use battery storage, which has been found to be effective when working in parallel with PV in peak load shaving. Time shifting renewable energy generation through the use of

Battery Energy Storage Systems (BESS) can reduce the operating cost. Many studies have been focused on optimal operation with PV and battery storage. However, while achieving this optimal operation for the generators is necessary, it does not ensure secure operation of power systems. Therefore, validating secure operation with optimal generation scheduling is important. Furthermore, disregarding the battery life in optimal power scheduling creates an unrealistic scenario since replacing the battery is costly.

In this research, a comprehensive study of a 40 MW PV penetration with battery storage to the Tabuk Grid is presented. The study includes complete simulation and analysis of the PV integration with storage. Moreover, a power quality study for the PV farm is conducted, one that included nonlinear loads to enhance the analysis regarding harmonics penetration. In addition, this research presents an optimal generation scheduling considering renewable energy sources, the BESS, battery life and short term outages. This will enables the system to respond and resolve outages quickly without affecting the optimal operation. The feasibility of the proposed approach is demonstrated on Tabuk system – an isolated northwest grid in Saudi Arabia.

DEDICATION

To my beloved parents, Thank you for your endless support

ACKNOWLEDGMENT

Firstly, thank to Allah for the blessing to complete my education journey. Also, a special and huge thank to Dr. Makram for the priceless support, guidance and advice during my research. I am really honored and grateful to work with a person like Dr. Makram, who has an abundant experience, knowledge, and professional academic career.

Secondly, I would like to thanks and express my gratitude to all my frindes in power group. And I wish them a successful life.

Finally, whatever I do I will not meet what they have done for me; They are my parents. So, a deep thanks to you for your prayers and support in all successes that I have accomplished in my life.

TABLE OF CONTENTS

Page

TITLE PAGE I

ABSTRACT II

DEDICATION IV

ACKNOWLEDGMENT V

LIST OF FIGUERS X

LIST OF TABLES XIII

CHAPTER 1 1

Electricity and Renewable Energy in Saudi Arabia 1

1.1 Introduction 1

1.2 Saudi Electricity Company 2

1.3 Future governmental plans and actions. 7

1.4 Solar Irradiation in Saudi Arabia 7

1.5 PV and Solar Project in the Kingdom. 12

1.6 Summary 15

1.7 Dissertation Outline 16

CHAPTER 2 17

PV Penetration with Battery Storage for an Isolated Northwest Grid of Saudi Arabia 17

2.1 Introduction 17

2.2 PSCAD Software 18

2.2.1 PV Cell Model in PSCAD 18

2.2.2 MPPT Model 21

2.2.3 Battery model 22

2.3 PV and Battery Model Control Scheme 25

Page

2.3.1 PV Model 25
2.3.2 Battery Model 28
2.4 Saudi Arabia National Grid 28
2.5 Simulation Result 31
2.6 Summary 37

CHAPTER 3 38
Power Quality Study of an Isolated Northwest Grid of Saudi Arabia with PV and Storage 38
3.1 Introduction 38
3.2 Filter Design 39
3.3 Nonlinear Load Model 40
3.4 Simulation Result. 41
3.5 Summary 46

CHAPTER 4 47
Optimal Operation of a Power System 47
4.1 Introduction 47
4.2 Classical Economic Dispatch 48
4.2.1 Input-Output Characteristic of Thermal Unit 48
4.2.2 ED Problem Formulation 50
4.3 Optimization Methods 51
4.4 Mixed Integer Quadratic Programming (MIQP) 52
4.4.1 Problem definition 53
4.4.2 Branch and Bound 54
4.5 Test System 56
4.6 Problem Formulation 57
4.6.1 Power Balance Equation 57
4.6.2 Generation Limits 57

Page

4.6.3 Fixed Cost for the Generator 57
4.6.4 Startup Cost 58
4.6.5 Objective Function 58
4.7 Simulation Result 58
4.8 Summary 62

CHAPTER 5 63
Secure Operation and Optimal Generation Scheduling Considering Battery Life 63
5.1 Introduction 63
5.2 PV Output Power 65
5.3 Battery Usage Cost 66
5.4 Problem Formulation 68
5.4.1 Energy Storage 68
5.4.2 Power Balance Equation 69
5.4.3 Generation Limits 69
5.4.4 Fixed Cost for the Generator 69
5.4.5 Startup Cost 70
5.4.6 Objective Function 70
5.5 Forced Contingency Analysis 70
5.6 Simulation Result 71
5.7 Summary 81

CHAPTER 6 82
Summary and General Conclusion 82
A. Objectives of Dissertation 82
B. General Conclusion 83
C. Contribution of the dissertation 85
D. Future Work 85

REFERENCES 86

Page

APPENDICES 94

APPENDIX A: Line and Load data. 95

APPENDIX B: Nomenclature 96

LIST OF FIGUERS

Page

Figure 1.1: Peak load in Saudi Arabia. 4

Figure 1.2: Generation capacity based on unit type. 5

Figure 1.3: Number of units based on unit type. 5

Figure 1.4: Load profile for the Kingdom for 2014. 6

Figure 1.5: Average daily GHI [12]. 10

Figure 1.6: Average daily DNI [12]. 10

Figure 1.7: Solar irradiation by station (Oct.2013-Semp.2014) [12]. 12

Figure 2.1: PV array (left) and MPPT (right). 18

Figure 2.2: PV cell equivalent circuit [17]. 19

Figure 2.3: Typical I-V characteristic of PV cell [17]. 19

Figure 2.4: PV array (left) and PV cell parameters (right). 20

Figure 2.5: Incremental conductance MPPT algorithm [17]. 21

Figure 2.6: Battery equivalent circuit [20]. 22

Figure 2.7: PSCAD custom battery component. 23

Figure 2.8: Battery model's configurations. 24

Figure 2.9: (a) Single line diagram of PV system. (b) PV control. (c) Battery control. ... 25

Figure 2.10: Operation areas [25]. 29

Figure 2.11: Substations locations. 30

Figure 2.12: Load profile for Tabuk. Solid line represent daily load, Dashes line the temperature. 31

Page

Figure 2.13: (a) PV and battery active power delivered to the grid. (b) Generation stations power..... 33
Figure 2.14: Battery SOC %. 33
Figure 2.15: Battery current for one farm. 34
Figure 2.16: Battery power. 35
Figure 2.17: THD of PV current. 35
Figure 2.18: Active and reactive power for one Farm. 36
Figure 2.19: dq-axis current for one farm. 36
Figure 3.1: Nonlinear load model. 40
Figure 3.2: Load current without filter of Bus 9. 42
Figure 3.3: THD at Bus 9. Figure 3.4: Harmonic component. 43
Figure 3.5: Load current with filter of Bus 9. 43
Figure 3.6: THD of load current at Buses 1 and 2. 43
Figure 3.7: THD of load current at Buses 3 and 4. 44
Figure 3.8: THD of load current at Buses 5 and 6. 44
Figure 3.9: THD of load current at Buses 7 and 8. 44
Figure 3.10: THD of load current at Buses 9 and 10. 45
Figure 3.11: THD of load current at Buses 11 and 12. 45
Figure 3.12: THD of PV current at PCC..... 46
Figure 4.1: Input output characteristic curve of a thermal unit..... 49
Figure 4.2: N thermal units supplying a load [48]. 51

Page

Figure 4.3: Binary search tree [50]. 55

Figure 4.4: Shows an example of using bounds to eliminate nodes [50]. 56

Figure 4.5: Scheduled power for Case C: (a) Tabuk-1 generators output, (b) Tabuk-2 generators output. 61

Figure 4.6: Scheduled power for Case D: (a) Tabuk-1 generators output, (b) Tabuk-2 generators output. 61

Figure 4.7: Supply and demand. 61

Figure 5.1: Irradiation data. Figure 5.2: PV output power..... 66

Figure 5.3: Simulation result for case C scenario1. 74

Figure 5.4: Simulation result for case D scenario 2. 75

Figure 5.5: Simulation result for case E scenario 2. 76

Figure 5.6: Simulation result for case B scenario1: (a) and (b) Battery usage cost included, (c) and (d) Battery usage cost excluded. 77

Figure 5.7: Simulation result for case A scenario 2: (a) and (b) Battery usage cost included, (c) and (d) Battery usage cost excluded. 78

Figure A. 1: Single line diagram of Tabuk grid. 95

LIST OF TABLES

Page

Table 1.1: shows the generation capacity for each provider [4]. 6

Table 1.2: Long-term daily mean values of sunshine duration and GSI on horizontal surface [8]. 9

Table 1.3: shows the solar projects initiated by the ERI at KACST [13]. 14

Table 2.1: Voltage level for each bus. 32

Table 2.2: Parameters of each PV array. 32

Table 3.1: Harmonic Number h(n) VS Individual Harmonic distortion [35]. 41

Table 3.2: Load current THD compared with the standard Limits. 45

Table 4.1: Shows all generators (diesel) capacity [58]. 59

Table 4.2: Standard IEEE coefficient for the fuel cost curve [59]. 59

Table 4.3: shows the optimal operation cost for Tabuk grid. 60

Table 5.1: Battery data and cost [74]. 67

Table 5.2: Shows battery constraints. 72

Table 5.3: shows the optimal operation cost for all the cases. 72

Table 5.4: Shows number of cycles performed for each case. 79

Table 5.5: Optimal generated power at peak loads for each case with PV and battery. ... 80

Table 5.6: Observed violation cases. 80

Table A. 1: Line and Peak load data. 95

CHAPTER 1

Electricity and Renewable Energy in Saudi Arabia

1.1 Introduction

Over the past three decades, the consumption of electricity in Saudi Arabia has increased significantly, with many studies suggesting that power demand in the kingdom will continue to increase for the next 15 years, reaching an estimated 120 GW by 2032 [6]. The evolution of industry and population growth are the primary factors contributing to this rapid increase in demand. Satisfying this increasing demand for power in the future requires significant changes in the Kingdom's power system, one important focus being integrating the use of renewable resources as an alternative to traditional power supplies. This initiative has received strong support from the government, specifically for the research and development of solar energy technology as well as for other forms of sustainable energy.

The geographical location of the Kingdom, the vast expanse of land, its lack of rainfall and the year-round clear sky all make the country an outstanding candidate for the application of large scale photovoltaic (PV) power farm, conditions potentially making Saudi Arabia one of the largest photovoltaic energy producer and exporter. In addition to eliminating fuel cost, PV power generation leads to cleaner energy and reduced maintenance and pollution. A more important contribution is the ability of large scale PVs to reduce oil consumption, significant as most power generation plants in the Kingdom currently use fossil fuel. Furthermore, as the increase in demand results in the burning of

more oil for power, the oil and gas exports will be affected, in turn impacting the country's economy.

1.2 Saudi Electricity Company

Until the mid-1970s, electricity was limited to the main cities and towns in Saudi Arabia. As this service was operated by local businesses and municipalities, the rates, quality, and customer satisfaction varied across the Kingdom. Between 1976 and 1985, the Kingdom combined almost these independent electricity providers into four major companies based on region (Eastern, Western, Central and Southern). However, private small firms still supplied electricity in the remote areas. In 1998, the government announced the merging of the four regional companies into the Saudi Electricity Company (SEC), which was formally established in 2002 with the government owning 74.3% of the stock. In addition, this announcement included the establishment of an independent energy authority to evaluate electricity rate and cost, resulting in the founding of the Electricity and Cogeneration Regulatory Authority (ECRA) in 2001. This agency is responsible for the planning and development of the power sector as well as ensuring that the investment in power generation for both the government and private sectors is sufficient for future projects and demand [1].

The peak load in Saudi Arabia has increased dramatically over the past 40 years; in 1975, the peak load was only 300 MW and the number of customers was 351,531 [2], while 39 years later the number of customers had increased to 7,602,279 and the total peak load to 56,827 MW [3]. As can be seen in Figure 1.1, the peak load more than doubled between 2004 and 2014. Some of the key factors that play a role in this increase in demand include

the rapid population expansion, the lower electricity rates and the high economic growth. These factors have led the Kingdom to expand its power capability and network to support its future industrial plans and load demands. As a result, the SEC initiated large projects throughout the country to address the future increase in power demand, upgrading the plants and expanding power production by increasing support to the electrical grid, improving turbine efficiency, and installing new units. Specifically, the company added three steam turbine units with a capacity of 2100 MW to the west sector, two steam turbine units with a capacity of 520 MW to the east sector and two gas turbine unites with a capacity of 128 MW to the south sector [3]. In addition, the private sector also contributed significantly to increase power production. As a result, by 2014, the SEC had increased power production to 214.589 GWh, an increase of 8% from the 198.9 GWh in 2013 [3].

Most of the power plants in Saudi Arabia are conventional fossil-fuel thermal units, with steam and gas turbine units providing the highest percentage of the actual generation capacity. In 2014, gas units provided 47% and steam units provided 40% of the total generation capacity in the Kingdom whereas the combined cycle and diesel units generated 12% and 1% respectively. Figure 1.2 shows the generation capacity based on the type of unit, and Figure 1.3 illustrates the number of units [4]. While the generation capacity in the Kingdom is mostly provided by the SEC, some private and governmental sectors also contribute to the network. Table 1.1 shows the generation capacity for each provider. In terms of the installed generation capacity, the EOA and WOA regions are the highest, with 37% and 35% of the total generation capacity, respectively, while COA and SOA generate 27% and 7%, respectively [4].

The peak load per year is dependent on the climate. The kingdom has only two seasons: summer and winter. Due to geographical location, the summer is intensely hot, with temperature reaching 50 degrees Centigrade in some areas. The winters are relatively milder, with the northern sections of the country experiencing colder weather than the other regions. Therefore, the peak load is higher in the summer than in the winter due to the heavy use of air conditioners, as illustrated in Figure 1.4 [5].

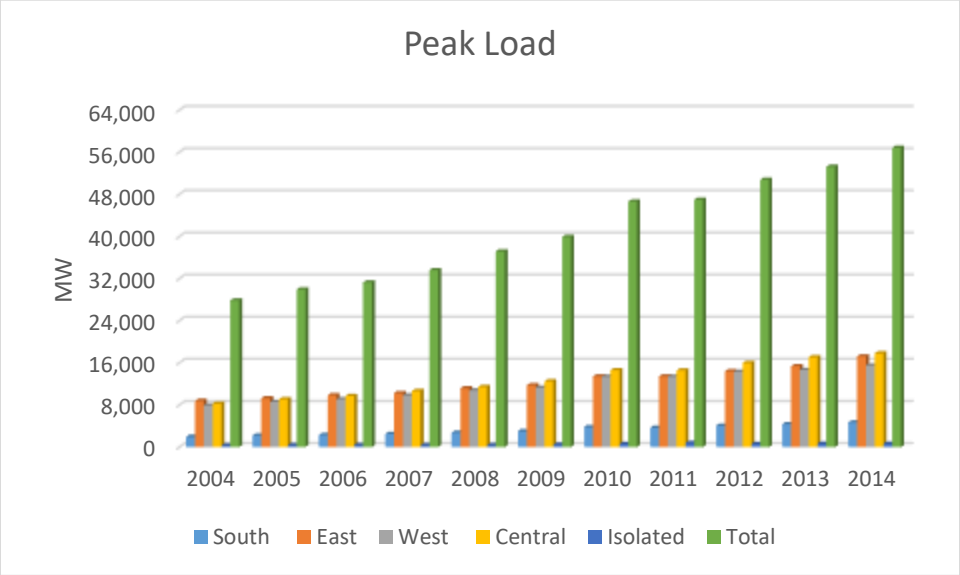

Figure 1.1: Peak load in Saudi Arabia.

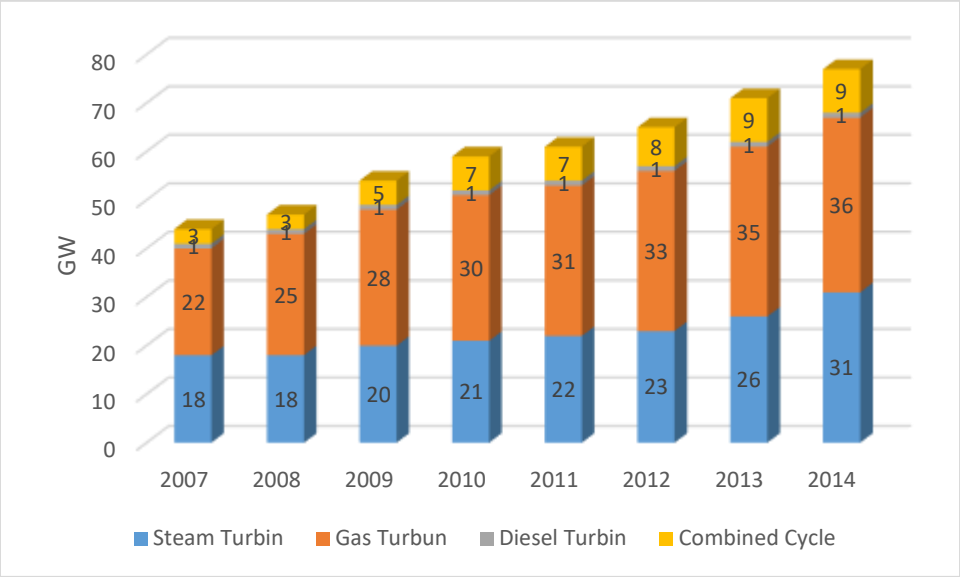

Figure 1.2: Generation capacity based on unit type.

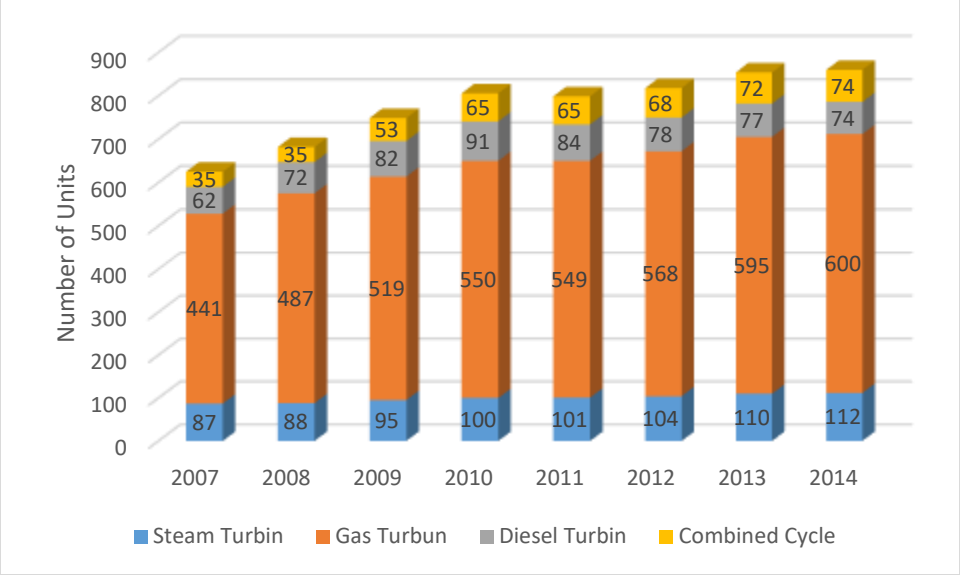

Figure 1.3: Number of units based on unit type.

Table 1.1: Shows the generation capacity for each provider [4].

Providers	**No. of Plants**	**Capacity MW**
Saudi Electricity Company	46	54,717
Saline Water Conversion Corporation, SWCC	6	4,761.60
Hajr for Electricity Production Company	1	3,415
Jubil Water & Power Company	1	2,875
Saudi Aramco	8	1,927
Durmah Electric company	1	1,756
Marafiq	1	1,589
Rabigh Electric Company	1	1,320
Shuaibah Water & Electricity Company	1	1,191
Tihama Power Generation Company	4	1,083
Shaqaiq Water & Electrical Company	1	1,020
Rabigh Arabian Water and Electricity	1	600
Jubil Energy Company	1	250
Saudi Sement Company	2	227
Tuwairqi Energy Company	1	74
Alaman Company	3	18
Obeikan Paper Industries Company	1	16
Total	80	76,839

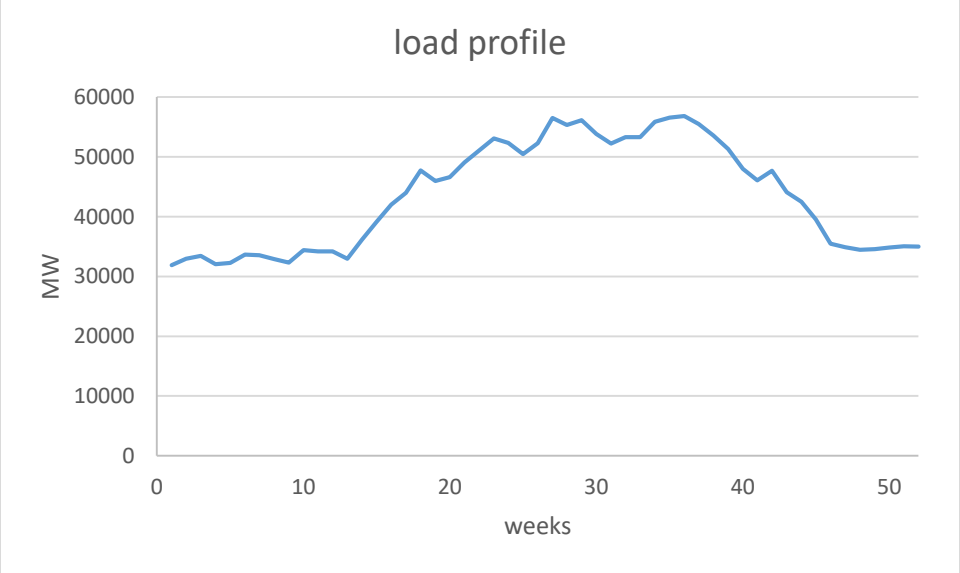

Figure 1.4: Load profile for the Kingdom for 2014.

1.3 Future governmental plans and actions.

Saudi Arabia faces a growing demand for energy as its population increases. According to governmental estimations, the expected demand for electricity will exceed 120 GW by 2032 [6]. In addition, the fossil fuel consumption for power, industry and transportation is expected to increase from 3.4 million barrels per day in 2010 to 8.3 million barrels per day in 2028 [6]; as a result, the oil and gas exports, approximately 90 % of the country's revenue, will be affected by this increased domestic consumption. Therefore, conservation and finding alternative sources of energy are vital for the Kingdom. This objective can be accomplished by employing renewable resources such as solar, wind and thermal. In order to explore these options in face of the country's energy challenges, the government has established the King Abdullah City for Atomic and Renewable Energy (K.A.CARE), its mission being to develop an energy program to meet this increasing demand, to develop a variety of sustainable renewable resources that can provide clean power that reduces pollution and protect the environment, and to protect the Kingdom's oil and gas resources for the future. While K.A.CAER concluded that fossil fuel will remain the primary fuel resources for meeting the 2032 demand, it plans to support it with a variety of renewable sources. Including solar energy, photovoltaic and consecrated solar power (CSP). More specifically, its plan calls for approximately 41 GW of solar, 16 GW of PV and 25GW of CSP [6].

1.4 Solar Irradiation in Saudi Arabia

Solar irradiation data are essential requirement for solar energy development. The first Saudi solar radiation atlas, introduced by the King Abduaziz City for Science and

Technology (KACST), covered these data for the period from 1971 to 1980. In 1987, a collaboration between KACST and the United State Department of Energy (DOE) in the field of renewable energy and research development resulted in 12 monitoring stations that provided solar radiation data for the Kingdom in 1993. More recently, the Renewable Resources Monitoring and Mapping Program (RRMM), a collaboration between KACARE and the National Renewable Energy Laboratory (NREL), began in 2013 [7].

The application of large-scale PV farms is feasible due to the geographical location and the size of Saudi Arabia. The country is located in what is referred to as the Sun Belt, the area receiving the most radiation on the planet. Table 1.2 shows the long-term mean value of the sunlight period and the global solar irradiation (GSI) at 41 sites in the kingdom [8]. Saudi Arabia has an average sunshine duration of approximately 8.89 hour per day and an average GSI of more than 2000 kWh/m^2 every year on a horizontal surface [8, 9]. The highest GSI values for European countries are not comparable with those observed in Table 1.2, meaning Saudi Arabia is in a good position to become one of the largest producer and exporter of solar energy. The development of solar energy in the country began in 1960, with the technology and research development being started in 1977 by KACST. In 1994 the atlas for solar radiation project was originated as a cooperative project between the Energy Research Institute (ERI) at KACST and the NREL [10]. Currently, the total solar energy generated at various locations in Saudi Arabia is about 22 MW, with another 111.8 MW under construction [11].

Table 1.2: Long-term daily mean values of sunshine duration and GSI on horizontal surface [8].

No.	Location	Hour	MWh/m^2 yr	No.	Location	Hour	MWh/m^2 yr
1	Qurayyat	9	2.03	22	Al-Kharj	9.1	2.03
2	Tabarjal	9	1.72	23	Harad	9	1.71
3	Sakaka	9	1.94	24	Yabrin	9.1	2.06
4	Tabuk	9.1	1.64	25	Al-Aflat	9	2.19
5	Tayma	9.2	2.04	26	Khulays	8.9	2.18
6	Hail	9.4	1.91	27	Sayl Kabir	8.9	2.46
7	Sarrar	8.7	1.66	28	Turbah	9	2.09
8	Al-Ula	9.1	2.12	29	Taif	8.9	1.98
9	Qatif	8.4	1.73	30	Sulayyil	9	2.4
10	Maaqala	8.9	1.78	31	Bisha	9.2	2.56
11	Zilfi	8.9	2.04	32	Heifa	9.1	2.22
12	Unayzah	9.3	2	33	Juarshy	8.5	1.98
13	Uqtalas-Suqur	9.1	2.23	34	Modaylif	8.5	2.32
14	Hutatsudair	9	2.15	35	Al-Numas	7.4	2.21
15	Al-Hofuf	8.7	2.07	36	Kwash	8.5	1.7
16	Shaqra	9.2	2.21	37	Kiyad	8.4	1.87
17	Hanakiya	9.1	2.21	38	Sirr-Lasan	8.7	1.84
18	Riyadh	9.2	1.87	39	Abha	8.7	2.13
19	Madina	9.1	2.32	40	Najran	9.1	2.53
20	Dawdami	8.8	2.17	41	Sabya	8.5	1.83
21	Derab	8.7	2.26				

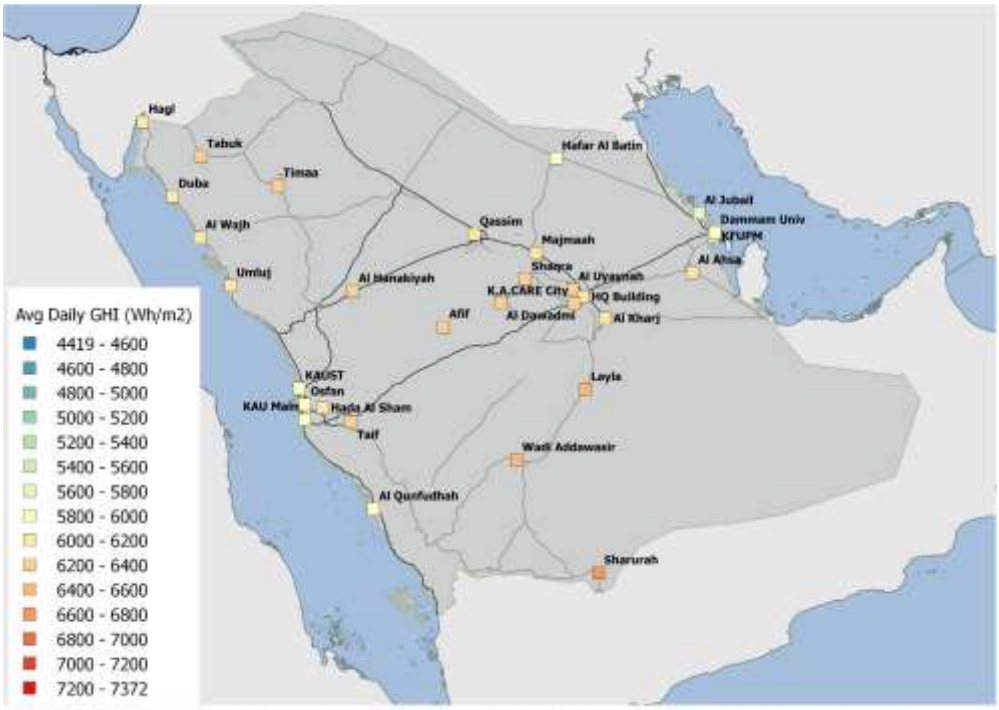

Figure 1.5: Average daily GHI [12].

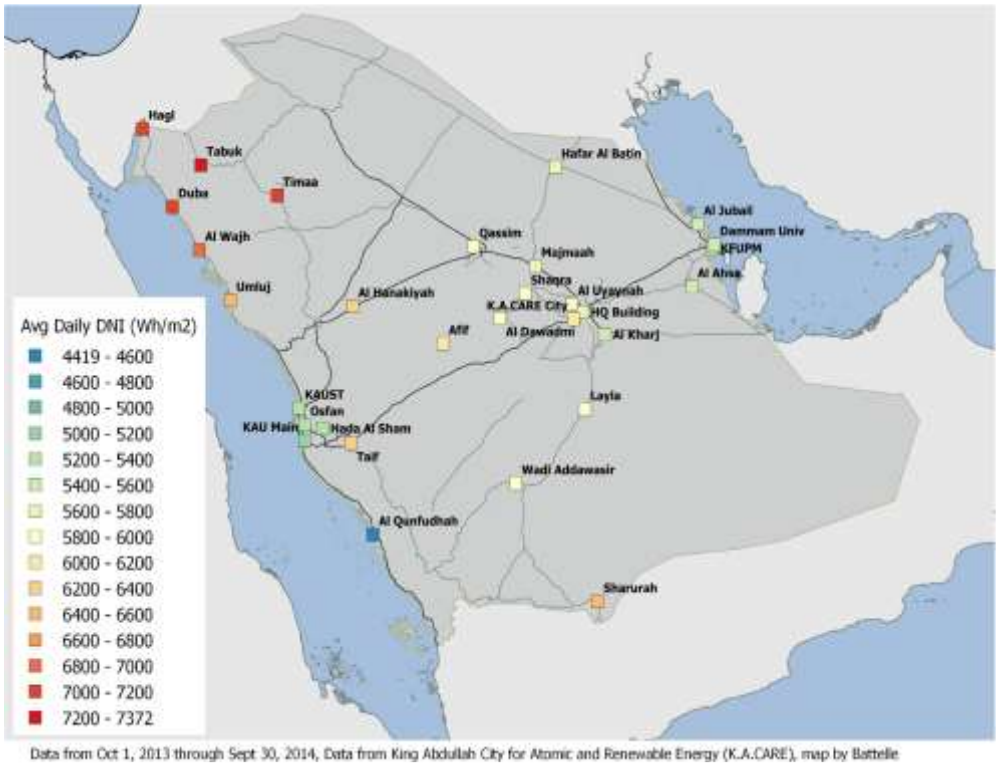

Figure 1.6: Average daily DNI [12].

The finding from a recent study conducted by K.A.CARE [12] on solar irradiation in the Kingdom indicates that photovoltaic technology perform well at any location in the country even in the areas subjected to extremely high temperatures. This study analyzed per minute measurement of Global Horizontal Irradiation (GHI), Direct Norm Irradiation (DNI) and Disuse Horizontal Irritation (DHI) for one year (October 2013 through September 2014) collected from 30 stations distributed across the country, The results indicating that the annual average daily GHI ranges between 5700 Wh/m^2 and 6700 Wh/m^2 with lower values observed over the coasts and higher ones a cross the upcountry. In addition, more variability in the annual average daily DNI was observed over all stations, ranging between 4400 Wh/m^2 and more than 7300 Wh/m^2 under clear skies, with higher values being detected in the northwest area. However, in terms of yearly average DNI, the western inland station locations exhibited higher values than the eastern sites at 2400 kWh/m^2/year and 2000 kWh/ m^2/year, respectively.

The study concluded that the northwestern section of Saudi Arabia represents the most promising area for initiating solar power projects because of its clear sky and high solar radiation. This study also indicated that the daily amount of vertical radiation of DNI exceeds 6500 Wh/m^2 in Hagl, Umluj, Duba, Al Wajh, Timaa and Tabuk, and increases up to 7372 Wh/m^2 in the summer. Furthermore, this study showed that coastal cities and regions experienced the least daily amount of DNI because of high humidity and fog [12].

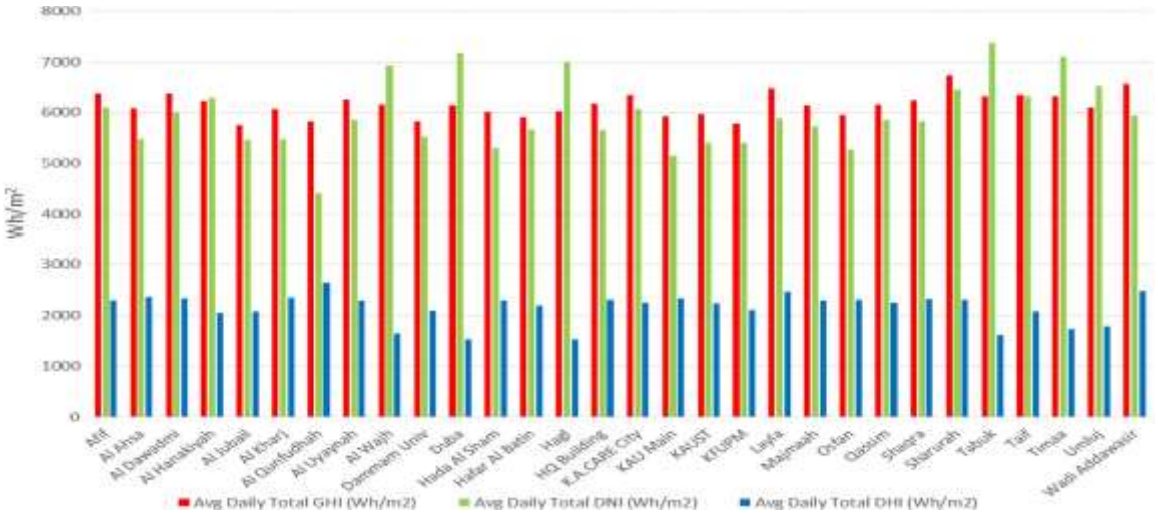

Figure 1.7: Solar irradiation by station (Oct.2013-Semp.2014) [12].

1.5 PV and Solar Project in the Kingdom.

In Saudi Arabia, the application of solar energy began in the 1960s, with much research and development in its applications being conducted by KACST in 1977, including significant collaborative efforts with the United States through SOLERAS and with Germany through HYSOLAR. The largest project constructed by SOLERAS was the solar village created between 1977 and 198. The aim of this project is to deliver electricity to three villages located nearby that were not connected to the regional grid. This solar village farm has a total peak output power of 350KW DC, with a 300 KVA inverter and 1100 kWh lead-acid battery storage device covering a space of 4000 m^2. The project, which was a completely automatic operation, is designed for either co-generation or stand-alone operational modes [13]. Table 1.3 shows the solar projects initiated by the ERI at KACST.

The government has continued its strong support of solar energy, completing additional projects. In 2010, the first large-scale PV installed in Saudi Arabia was the rooftop solar

park at King Abdullah University of Science and Technology near Jeddah with a total power of 2MW. Another project, the Saudi Aramco Solar Park designed by Aramco in Dhahran in 2011, has a capacity of 10 MW. The next year, in 2012 a solar farm with a 3.5MW peak power generation capacity was lunched at King Adullah Petroleum Studies and Research Center in Riyadh. Finally, the world's largest thermal plant at Princess Noura University in Riyadh provides more than 900,000 liters of hot water storage. The plant includes 36,305 square meters of solar panels that inject solar energy into a district heating grid for 40,000 students [14].

Table 1.3: Shows the solar projects initiated by the ERI at KACST [13].

Projects	**Location**	**Duration**	**Applications**
350 kW PV system (2155 MWh)	Solar Village	1981–87	AC/DC electricity for remote areas
350 kW PV hydrogen production plant (1.6 MWh)	Solar Village	1987–93	Demonstration plant for solar hydrogen production
Solar cooling	Saudi universities	1981–87	Developing of solar cooling laboratory
1 kW solar hydrogen generator (20–30 kWh)	Solar Village	1989–93	Hydrogen production, testing and measurement (laboratory scale)
2 kW solar hydrogen (50 kWh)	KAU, Jeddah	1986–91	Testing of different electrode materials for solar hydrogen plant
3 kW PV test system	Solar Village	1987–90	Demonstration of climatic effects
4 kW PV system	Southern regions	1996	AC/DC electricity for remote areas
6 kW PV system	Solar Village	1996–98	PV grid connection
PV water desalination (0.6 m3 per hour)	Sadous Village	1994–99	PV/RO interface
Solar-thermal desalination	Solar Village	1996-97	Solar distillation of brackish water
PV in agriculture (4 kWp)	Muzahmia	1996	AC/DC grid connected
Long-term performance of PV (3 kW)	Solar Village	Since 1990	Performance evaluation
Fuel cell development (100–1000 W)	Solar Village	1993-2000	Hydrogen utilization
Internal combustion engine (ICE)	Solar Village	1993–95	Hydrogen utilization
Solar radiation measurement	12 stations	1994–2000	Saudi solar atlas
Wind energy measurement	5 stations	1994–2000	Saudi solar atlas

1.6 Summary

This chapter provides an overview of the history of electricity and renewable energy in the Kingdom. In addition, it includes the government's vision for addressing the increasing demand for power by employing renewable resources. The electricity services developed by establishing the SEC in 2002 and the independent energy authority, the ECRA, to evaluate the electricity cost and rates, and to plan the power sector to ensure that the grid is sufficient for future demand. Past research and development regarding solar energy indicate that the application of large-scale PV farms is feasible due to the geographical location and the large area of Saudi Arabia. Moreover, they shows that the most effective area for implementing solar power projects is the northwestern sections of Saudi Arabia, the Tabuk Region, due to its clear sky and the high solar irradiation.

1.7 Dissertation Outline

The work completed in each chapter is summarized as follows:

- **Chapter 1:** Provide an overview about the history of electricity and the renewable energy in the Saudi Arabia. Also, it gives the kingdoms' vision to overcome the increasing demand by employing renewable resources.
- **Chapter 2:** A brief description for the Kingdom's grid has been provided. A complete study of PV and battery storage penetration is presented.
- **Chapter 3:** This chapter presents a complete study of power quality for the isolated northwest grid of Saudi Arabia. Moreover, a combination of nonlinear loads are introduced for further analysis.
- **Chapter 4:** The classical method of economic dispatich (ED) is described and optimization techniques have been introduced. Moreover, the problem formulation of the Mixed Integer Quadratiq Programming (MIQP) is presented.
- **Chapter 5:** This chapter presents a secure operation and optimal generation scheduling while considering renewable energy sources and battery storage devices. It also achieves optimal operation considering battery life and short term outages.
- **Chapter 6:** Summaries and provides general conclusion of the dissertation and future work.

CHAPTER 2

PV Penetration with Battery Storage for an Isolated Northwest Grid of Saudi Arabia

2.1 Introduction

Renewable energy is an area of research of increasing importance because clean power sources have become environmentally essential in reducing the pollution produced from burning fossil fuels. One such simple and reliable renewable source of energy is Photovoltaic (PV): it can generate clean power, is readily available and lasts for long time. Due to environmental awareness and climate change, this energy source has experienced rapid growth, ranging from providing electricity for remote communities in an island mode or supporting utilities at peak load and load shaving in grid connected mode [15].

Photovoltaic is especially attractive to a country such as the Kingdom of Saudi Arabia, which is facing a high demand for energy expected to exceed 120 GW by 2032. The Kingdom which plans to have 41 GW of solar energy by 2032, has a high irradiation rates especially in the northwest area. According to the Renewable Resources Monitoring and Mapping Program (RRMM), the stations having the highest direct norm irradiation reading for July 2014 are located in northwest of Saudi Arabia, Tabuk region, with an daily average above 9000 Wh/m^2 [16]. Therefore, this area worth consideration for PV installation. A comprehensive study of integrating 40 MW PV with battery storage to Tabuk Grid is conducted in this chapter. The grid data were provided by the Saudi Electricity Company (SEC) Tabuk Branch.

2.2 PSCAD Software

PSCAD is one of the most efficient simulators that has been used for designing and modeling of power system components. The PV and Battery models in PSCAD are used for this study.

2.2.1 PV Cell Model in PSCAD

The PV model provided by the PSCAD technical and support teams was developed by Dr. A. Rajapakse at university of Manitoba, Canada. This model offers two components in the custom library of PSCAD, the PV array and the maximum power point tracking (MPPT) as shown in Figure 2.1. The equivalent circuit shown in Figure 2.2 that consisting of a current source in parallel with a diode, shunt and series resistance was used to describe and model the solar cell used here [17]. When the sun light falls on the cell, a DC current is generated, changing linearly with the solar irradiation. Solar cells are characterized by their nonlinear I-V curve, a typical one being shown in Figure 2.3. This nonlinear relationship is caused by the current I_d passing through the diode. A basic equation can be obtained by considering the equivalent circuit of the PV cell to describe the solar cell I-V relationship.

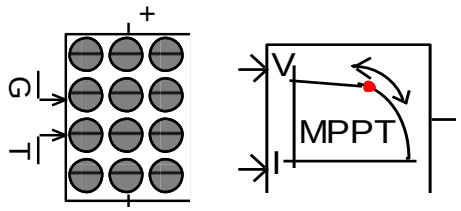

Figure 2.1: PV array (left) and MPPT (right).

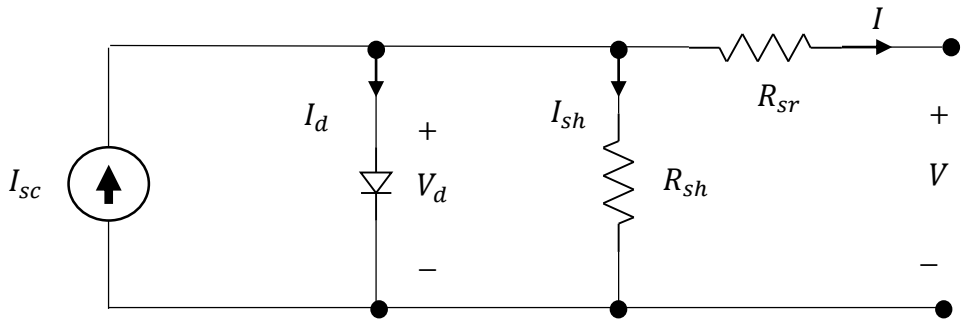

Figure 2.2: PV cell equivalent circuit [17].

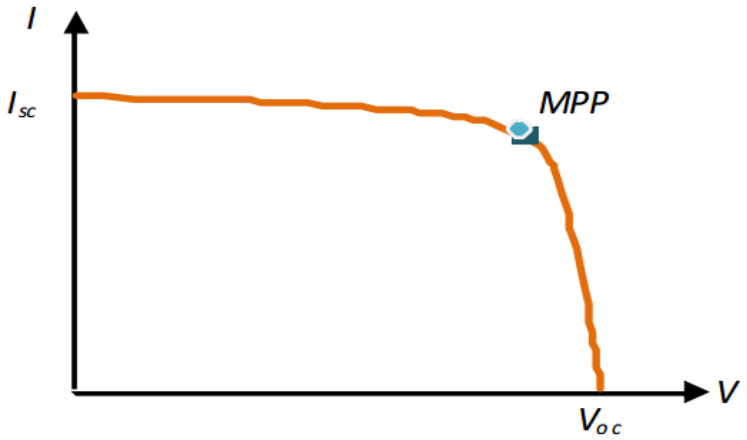

Figure 2.3: Typical I-V characteristic of PV cell [17].

The following equation is achieved by applying the Kirchhoff's law to the circuit [17]:

$$I = I_{sc} - I_d - I_{sh} \qquad (2.1)$$

By substituting the equivalent diode expression for I_d and the shunt branch current I_{sh}, Equation (2.1) becomes

$$I = I_{sc} - I_o \left[\exp\left(\frac{v+IR_{sr}}{\frac{nkT_c}{q}}\right) - 1\right] - \left(\frac{V+IR_{sr}}{R_{sh}}\right) \qquad (2.2)$$

where I_{sc} is the photo current which is a function of the cell temperature T_c and the solar irradiation G. The I_{sc} expression is represented as follows:

$$I_{sc} = I_{scr}\frac{G}{G_R}[1 + \alpha_T(T_c - T_{cR}) \qquad (2.3)$$

where I_{scR} is the short circuit current at the reference irradiation G_R and the reference temperature T_{cR}. α_T is the temperature coefficient of the photo current, I_o in Equation 2.2, which called the dark current, is a function of cell temperature and given by equation 2.4:

$$I_o = I_{oR}\left(\frac{T_c^3}{T_{cR}^3}\right)\exp[\left(\frac{1}{T_{cR}} - \frac{1}{T_c}\right)\frac{qe_g}{nk}] \qquad (2.4)$$

where I_{oR} is the dark current at the reference temperature, q the electron charge, k the Boltzmann constant, e_g the band gab energy of the solar cell and n the diode ideality factor.

A PV array is a combination of series and parallel modules, with a cell circuit that can be scaled up to characterize any such combination. Figure 2.4 shows the default PV array and PV cell parameters in PSCAD Library:

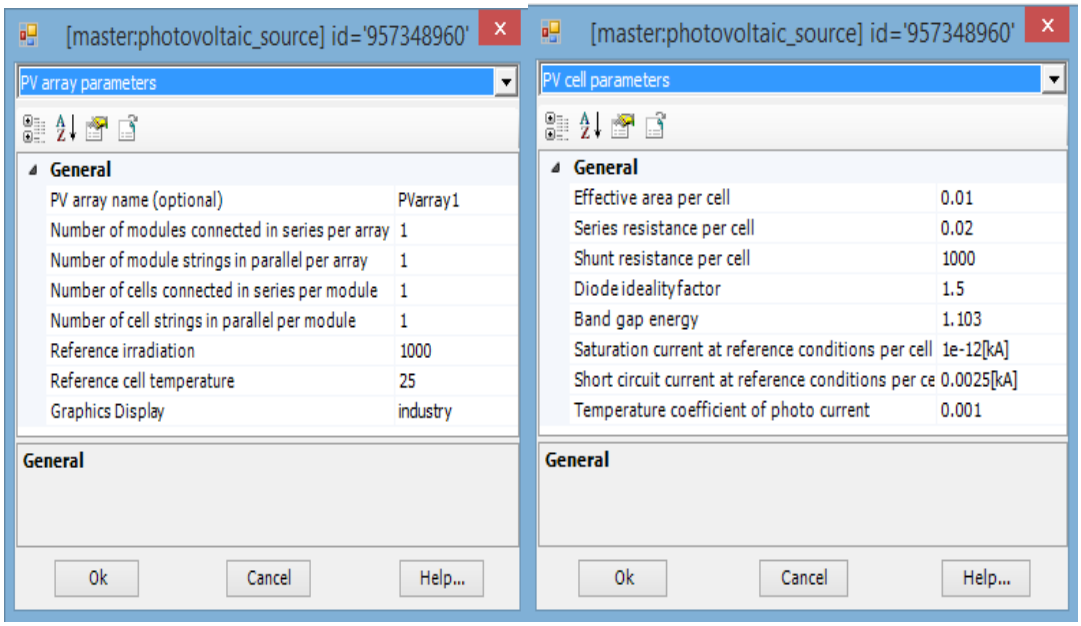

Figure 2.4: PV array (left) and PV cell parameters (right).

2.2.2 MPPT Model

The amount of power obtained by a PV array depends on the I-V curve as shown in Figure 2.3. To have maximum power drawn, it is required to operate at the optimal operation point at all the time, this point being the knee point of the I-V curve. MPPT is a DC-DC converter used to ensure achieving the optimal operating condition for the PV array despite varying load, temperature and irradiation. Figure 2.1 shows the custom library component developed for MPPT in PSCAD. Although MPPT involves several algorithms, a common one is the Perturb and Observe (P&O), which, however, has some restrictions. Another widespread algorithm is the Incremental Conductance Method (INC), which has several advantages over the P&O algorithm, including that it stops when it reaches the maximum power point without fluctuating around this value. In addition, it exhibits a higher degree of accuracy than the P&O under rapidly changing irradiation condition [18]. However, the INC leads to oscillations and work unpredictably during a highly altering atmospheric circumstances. Moreover, due to its complexity, the computation time increases and the sampling frequency slows down [19].

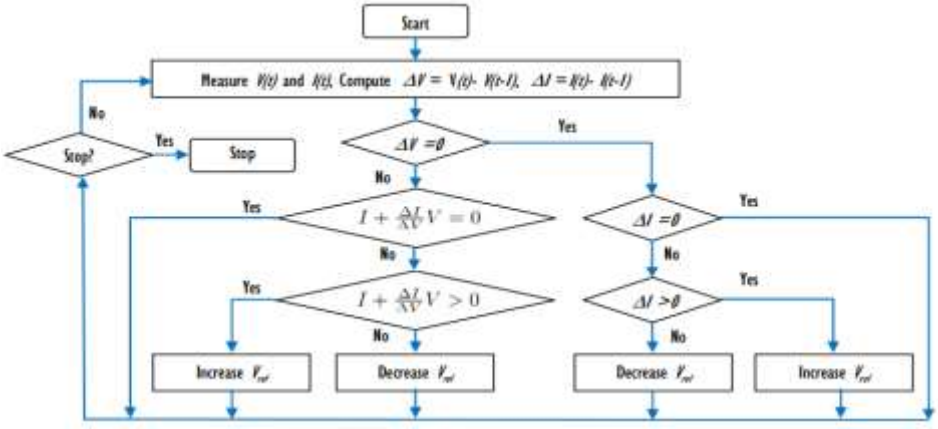

Figure 2.5: Incremental conductance MPPT algorithm [17].

2.2.3 Battery model

Because the output power of the PV fluctuates instantly as the amount of daylight falling on the panels changes, a battery bank is necessary to address the lack of solar power in cloudy weather and during the night. There are four common types of rechargeable batteries used to store the energy: Lead Acid, Nickel-51Cadmium (NiCD), Nickel-metal-hydride (NiMH), Lithium-ion (Li-ion), with Lead Acid being the ideal battery type for PV systems because of its low cost and its tolerance to overcharging.

The PSCAD battery model used for this research is based on Shepherd's equation for representing the electromechanical performance of a battery [20]. It is modeled using a controlled voltage source with a constant series resistance as shown in Figure 2.6.

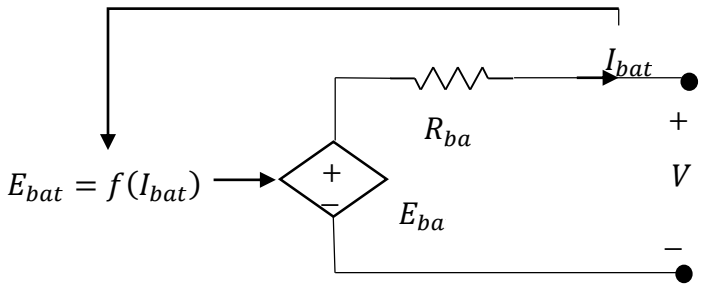

Figure 2.6: Battery equivalent circuit [20].

The battery equivalent circuit is represented as follows:

$$E_{bat} = E_o - k\frac{1-SOC}{SOC}Q + Ae^{-B(1-SOC)Q} \quad (2.5)$$

$$V_{bat} = E_{bat} - R_{bat}.I_{bat} \quad (2.6)$$

where:

E_{bat}: Internal Voltage.

E_o : Battery Voltage Constant.

SOC: State of Charge.

K: Polarization Constant (V/Ah)

Q: Battery Capacity (Ah).

A: Exponential Zone Amplitude (V).

B: Exponential Zone Time Constant Inverse (1/Ah).

V_{bat}: Terminal Voltage (V).

R_{bat}: Internal Resistance (ohm).

I_{bat}: Battery Current (A).

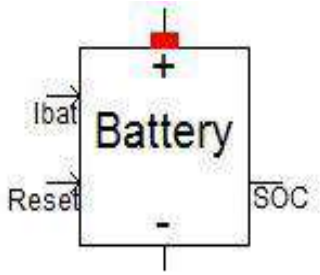

Figure 2.7: PSCAD custom battery component.

The battery model component in PSCAD master library is shown in Figure 2.7. The input signals include the battery current and the control signal for charging and discharging, while the output signal is the state of charge. Moreover, this model includes four types of batteries as well as user-defined model, as shown in Figure 2.8, allowing the user to define the characteristic of voltage vs SOC and the internal resistance vs SOC.

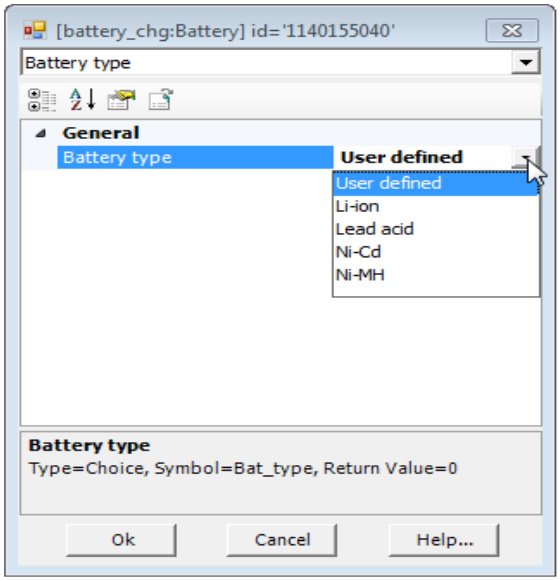

Figure 2.8: Battery model's configurations.

2.3 PV and Battery Model Control Scheme

Figure 2.9 shows the control scheme of a PV grid connected with Battery storage.

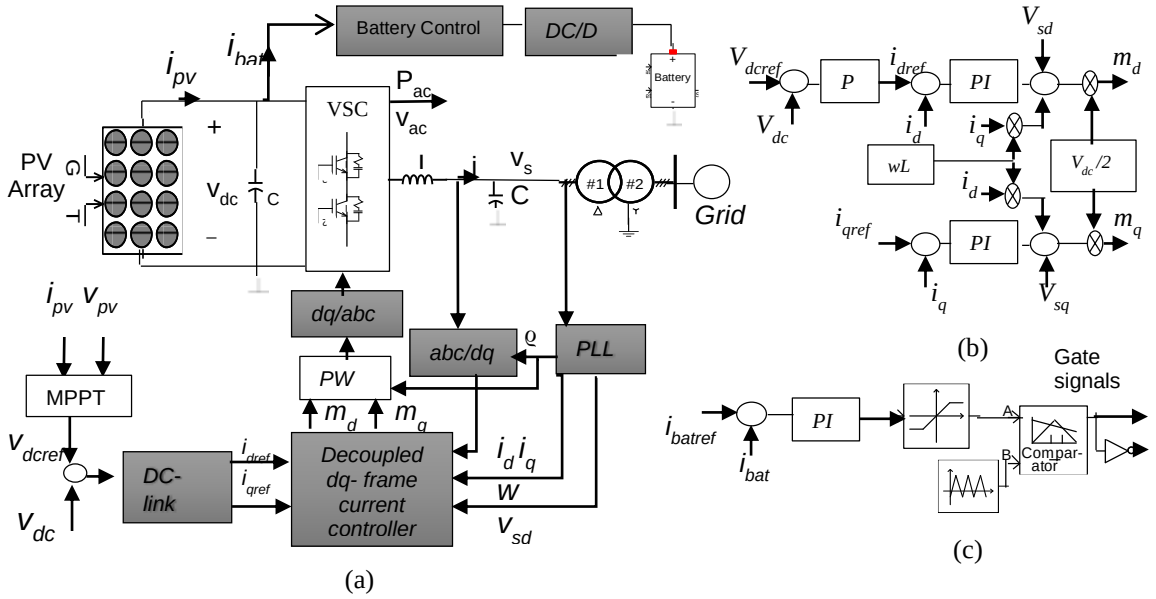

Figure 2.9: (a) Single line diagram of PV system. (b) PV control. (c) Battery control.

2.3.1 PV Model

Figure 2.9a is a schematic of a three phase grid connected PV system with battery storage consisting of a PV array, an inverter and a three phase reactor connected in series with the ac terminal of the inverter. The PV array is connected in parallel to the dc link capacitor and the dc terminal of the inverter. The inverter is controlled using a voltage source converter (VSC) modulation strategy based on sinusoidal pulse width modulation (S-PWM). The primary component of the PV array is the solar cell, which generates little power. To increase the output voltage and power, single cells are connected both in series and in parallel to form a module, meaning a PV array is the combination of parallel *Np* module and series *Ns* module needed to generate the required voltage and current output.

The capacitor C_f is used to reduce the harmonic produced by the PV system. Synchronizing the VSC and control to the grid voltage is achieved through a phase-locked loop (PLL) as shown in Figure 2.9 (a). In addition, the error between the V_{dc} reference given by the MPPT and the dc-link voltage is passed through a PI compensator whose output provides the d-axis reference current (i_{dref}). Then, the *dq*-frame current loop control is fed by i_{dref} to force d-axis current to track the i_{dref} to control the PV output power; to achieve a unity power factor the q-axis reference current i_{qref} is set to zero [21].

2.3.1.1 Phase Locked Loop

The PLL is used to synchronize the VSC's output voltage with electric-grid angular frequency to ensure the *dq*-frame transformed variables remains constant. By adjusting the q-axis reference voltage (v_{sq}) to zero, the PV system's active and reactive power are controlled as follows:

$$P = \frac{3}{2}\, v_{sd} i_d \qquad (2.7)$$

$$Q = -\frac{3}{2}\, v_{sd} i_q \qquad (2.8)$$

From (2.7) and (2.8), controlling the active power is achieved by regulating i_d and the reactive power is controlled by regulating i_q.

2.3.1.2 Voltage Control

The control of the dc voltage link is achieved by simply comparing the dc voltage with the reference value calculated from MPPT strategy to ensure that the PV works at its maximum output power. The error between these two signals is passed through a PI

compensator whose output provide i_{dref} , the input for the current controller as shown in Figure 2.9b. i_{qref} is set to zero to achieve the unity power factor.

2.3.1.3 Current Controller

The current controller compares the *dq*-reference currents with the actual ones to obtain the modulation signals(m_d, m_q). The control scheme is achieved by

$$L\frac{di_d}{dt} = -Ri_d + Lwi_q + \frac{v_{dc}}{2}\, m_d - v_{sd} \qquad (2.9)$$

$$L\frac{di_q}{dt} = -Ri_q - Lwi_d + \frac{v_{dc}}{2}\, m_q - v_{sq} \qquad (2.10)$$

The state variables of (2.9) and (2.10) are i_d and i_q while the input control signals are m_d and m_q and v_{sd} and v_{sq} are disturbance inputs. The *d-q* frame dynamics are coupled and nonlinear due to the *Lw* term. Hence, they must be linearized according to the following control principals [22]:

$$m_d = \frac{2}{v_{dc}}(u_d - Lwi_q + v_{sd}) \qquad (2.11)$$

$$m_q = \frac{2}{v_{dc}}(u_q + Lwi_d + v_{sq}) \qquad (2.12)$$

By substituting (2.11) and (212) into (2.9) and (2.10), two control inputs are produced which can control i_d and i_q independently, as follows:

$$L\frac{di_d}{dt} = -Ri_d + u_d \qquad (2.13)$$

$$L\frac{di_q}{dt} = -Ri_q + u_q \qquad (2.14)$$

However, m_d and m_q signals are converted back to the *abc* reference-frame to generate

the reference signals for the VSC. These reference waveforms are compared with triangular carriers to generate the pulsing signals to modulate the VSC [22].

2.3.2 Battery Model

As previously mentioned this study used the developed battery model in PSCAD [20]. Details of this battery model is described in [23]. It is modeled by a control voltage source with a series resistance. The charging and discharging process is controlled by constant current charging mode, with positive current reference for controlling charging process and negative reference for controlling discharging process. When the battery reaches a specific level of state of charge (SOC), the reference current is set to zero to maintain the voltage at that level. In Figure 2.9c, the DC/DC converter is operating in the current control mode, and the error signal is passed through a limiter, subsequently being compared with a triangular wave carrier to generate the pulse signals for the converter [24].

2.4 Saudi Arabia National Grid

As shown in Figure 2.10, the national grid of Saudi Arabia is divided into four operational areas: the Western Operation Area (WOA), the Southern Operation Area (SOA), the Eastern Operation Area (EOA) and the Central Operation Area (COA), each with its own network control center. These four areas are currently involved in interconnection projects, with the EOA grid is interconnected with the Gulf countries (GCC) and a connection with Egypt is under progress [25]. This interconnection is aiming to improve the grid, increase generation capacity, reduce operation cost and help meet load demand.

The total generation capacity in the Kingdom was 69.761 GW in 2013, with the SEC supplying 74% and the remaining from the Saline Water Conversion Corporation, the Jubil Company for Water and Electricity, and the Private Sectors with 7%, 4% and 15% respectively. Every year the power grid continues to expand in order to serve and deliver power to the increasing number of customers resulting from population growth and the increase in industrial sectors. More specifically, from 2004 to 2014, the peak load has more than doubled, jumping from 27.847GW to 56.827 GW as seen in Figure 1.1. The SOA has the lowest consumption of power, while the other three areas experiencing almost equal demand. Because of the increasing consumption, every year the power company has added more generation plants, resulting in a total of 76 plants by 2013. The map in Figure 2.10 indicates the different types of plant found throughout the Kingdom [26, 27].

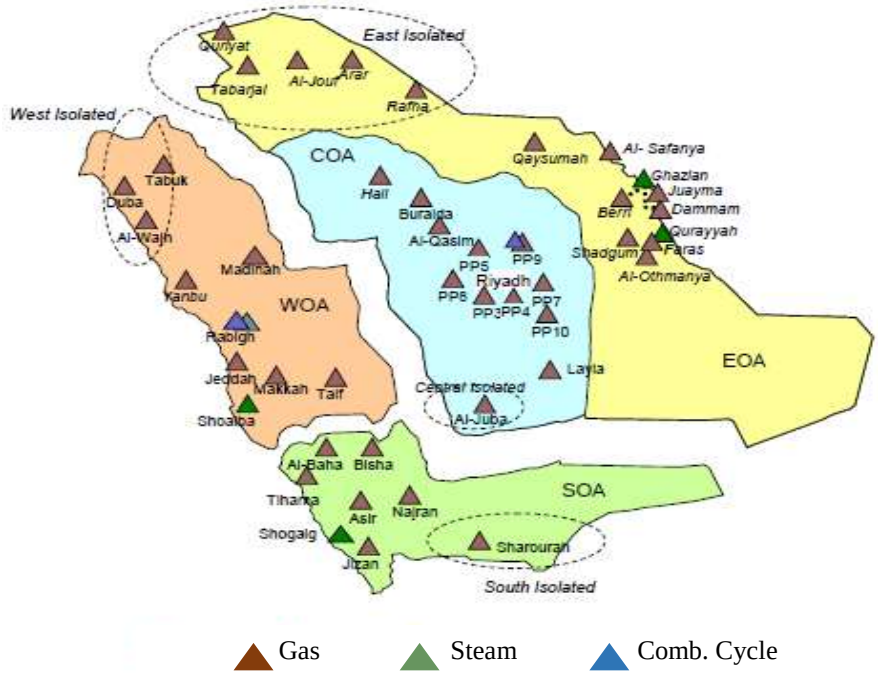

Figure 2.10: Operation areas [25].

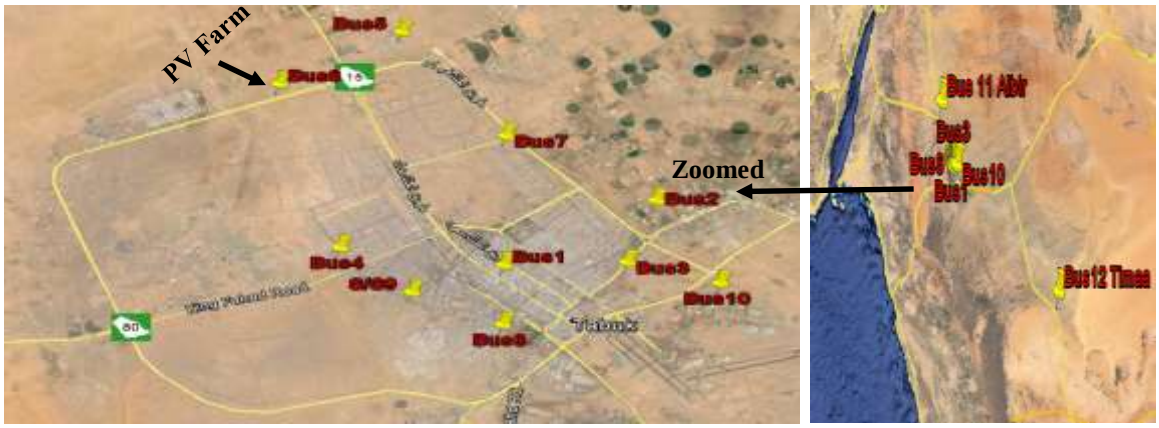

Figure 2.11: Substations locations.

The WOA consists of two areas as shown in Figure 2.10, the western section and the isolated northwest area, which includes Tabuk the capital of the region, and its sounding cities of Dubah and Alwajh. These cities are not interconnected, each having its own power generation. Tabuk is located in the far northwest of Saudi Arabia with a population more than 770,000 people [28]. According to the data provided from the SEC, Tabuk branch. As shown in Figure 2.11, the grid consists of 12 buses, with a voltage level of 132 KV. Table A.1 in Appendix A shows the lines and peak load data. The longest lines are those connecting Albir and Timma, distances of 60 km north and 237 km south, respectively. Other buses are distributed around the city as shown in Figure 2.11 as well as generation stations located at Bus 1 and 5 with a capacity of 102 MW and 857.2 MW, respectively [26]. Figure 2.12, which gives an overview of the power consumption in the city, shows the load profile for a summer and winter day

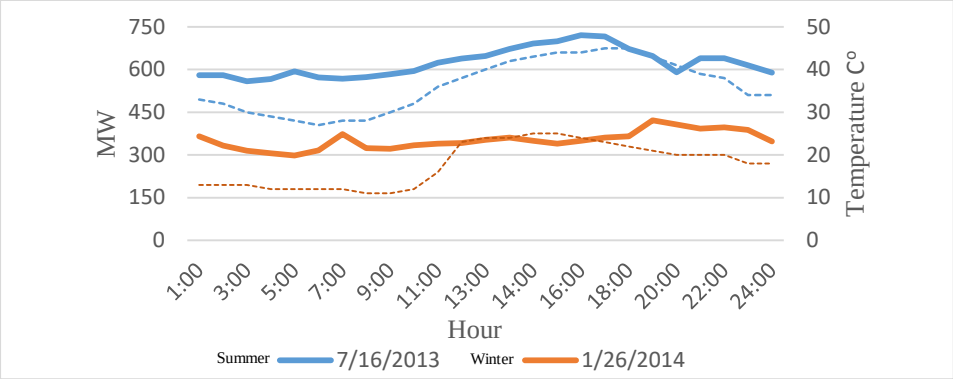

Figure 2.12: Load profile for Tabuk. Solid line represent daily load, Dashes line the temperature.

2.5 Simulation Result

The grid was built in PSCAD software, including a detailed model of the PV and the battery storage. During the simulation, a specific day, July 16.2013, was used for the peak loading condition, which was occurred at 4p.m. with a total of 720 MW being consumed. Bus 5 was selected as the slack bus for the system since it has the largest generation capacity. Table 2.1 shows the voltage level from the resulting power flow and the peak load at each bus. As this table shows, all voltages are within the limits. Because of its size, the PV farm needs to be located on available land outside of residential areas. An ideal area for the farm is close to Substation 6 as this land can accommodate two PV farms connected in parallel with a maximum generated capacity of 40 MW, 20 MW each. The parameters of each PV array are shown in Table 2.2. The battery storage, which is connected in parallel to the PV DC terminal, assumed to have a capacity of 50% of the total PV power. The initial irradiation applied to the PV is 1000 W/m^2 and the initial SOC for the battery is 70%. Figure 2.13a shows the different stages for the PV and battery penetration into the grid. First, max PV power of approximately 40 MW is delivered to the grid. At 3 seconds, a

charging process is initiated with half of the dc power being delivered to the battery bank. After the battery bank reaches 80 % SOC, the charging process stops, and the SOC is kept constant by setting the battery reference current to zero as shown in Figure 2.14. At 18 seconds, the battery begins to discharge to hold a total power of 60 MW from both the PV and the battery. Finally, during the discharging process, various irradiations are applied to the system, dropping to 750 W/m^2 at 25 seconds and to 500 W/m^2 at 30 seconds. Figure 2.13b shows the changes in output power of Station 1 to balance the generation for all stages of PV penetration with battery.

Table 2.1: Voltage level for each bus.

Bus	**V magnitude Pu**	**Angle Degree**	**Load at Peak MW**
1	1.03	-1.85	106
2	1.016	-1.88	94
3	1.015	-2.056	55
4	1.02	-1.79	62
5	1.04	0	11
6	1.027	-1.11	37
7	1.023	-1.422	60
8	1.015	-2.151	67
9	1.018	-1.909	134
10	1.014	-2.123	12
11	0.983	-3.935	33
12	0.97	-19.819	43

Table 2.2: Parameters of each PV array.

No. of series module per array.	170
No. of parallel module per array.	700
No. of series cells per module.	36
Cell’s short circuit current.	8.03 A
Cell’s open circuit voltage.	0.92 V
Array short circuit current.	5.621 KA
Array open circuit voltage.	5.630 KV
Current at P_{max}	5.295 KA
Voltage at P_{max}	3.81 KV

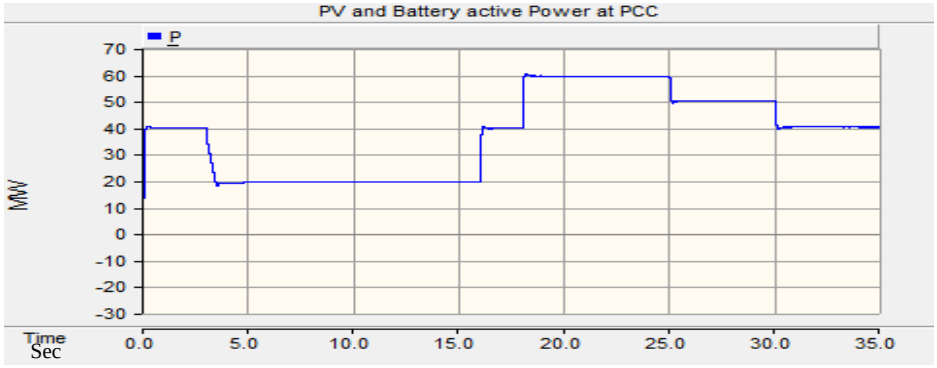

(a)

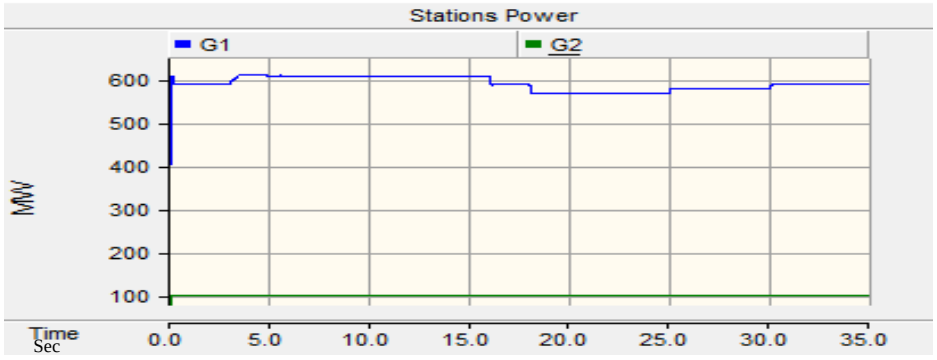

(b)

Figure 2.13: (a) PV and battery active power delivered to the grid. (b) Generation stations power.

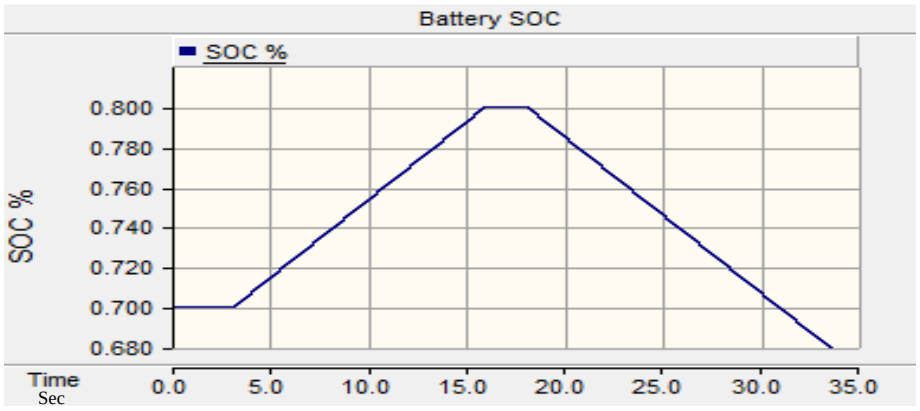

Figure 2.14: Battery SOC %.

One of the advantage of the battery model in PSCAD is that it allows the user to define the characteristic charge and discharge curves. Since the PV farm output power and the dc voltage are high, it is difficult to find a battery with an appropriate voltage level. Therefore,

a characteristic charge and discharge curve of a lead acid battery has been scaled up to match the DC link voltage and power. For the control scheme, the reference current for the battery can also be obtained based on the DC link voltage and the amount of power to be stored. Since the battery is assumed to have 50% of the PV power, the battery reference current is calculated as follows:

$$I_{batref} = \frac{PV_{power}\, x\, 50\%}{V_{dc}} \qquad (2.15)$$

As Figure 2.15 below indicates, the battery current follows the reference for both the charging and discharging modes; for the discharge process a negative reference is applied. In addition, when the SOC of the battery reaches 80%, the reference current is set to zero to keep the SOC constant as seen in Figure 2.14. The charging and discharging battery power is shown in Figure 2.16.

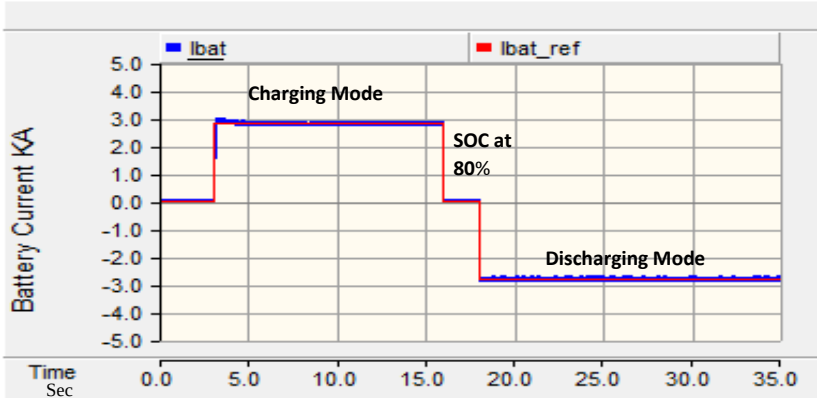

Figure 2.15: Battery current for one farm.

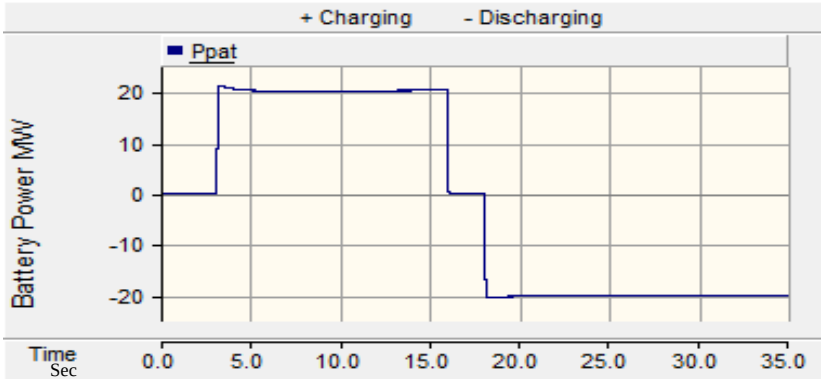

Figure 2.16: Battery power.

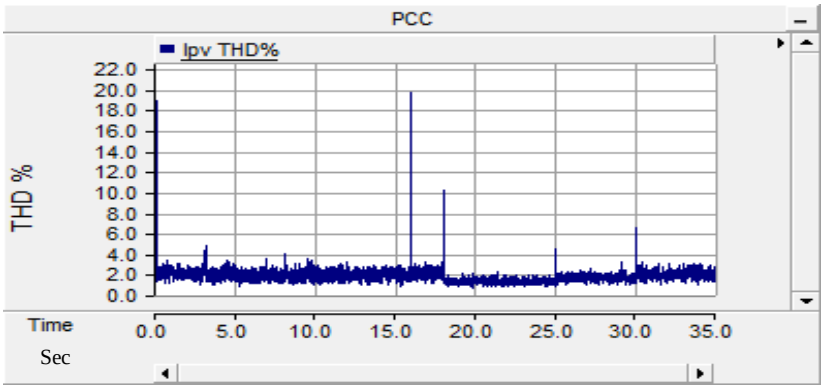

Figure 2.17: THD of PV current.

Figure 2.17 shows the THD for Phase A of the PV current injected into the grid during all stages. As can be seen, the THD oscillates around 2%, which is within the limit. In addition, the figure shows the two high values at the second 16 and 18 are instantaneous due to the switching of the reference current of the battery to keep the SOC at 80% and to begin the discharging mode. As Figure 2.18, a unity power factor is achieved for each farm by setting the *q*-axis current reference, which is responsible for controlling the reactive power, to zero. Figure 2.19, which illustrates the response of the *dq*-axis current, shows the

changes occurring to the *d*-axis current during all stages. The *q*-axis shows more fluctuation around zero when the discharging process began.

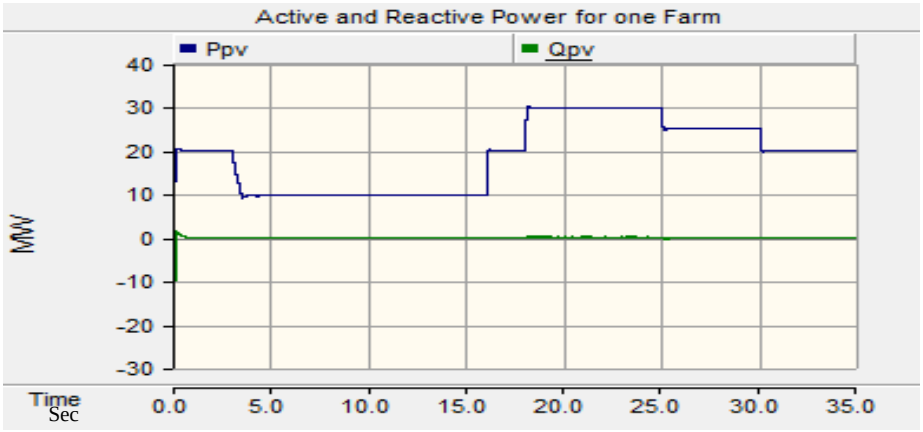

Figure 2.18: Active and reactive power for one Farm.

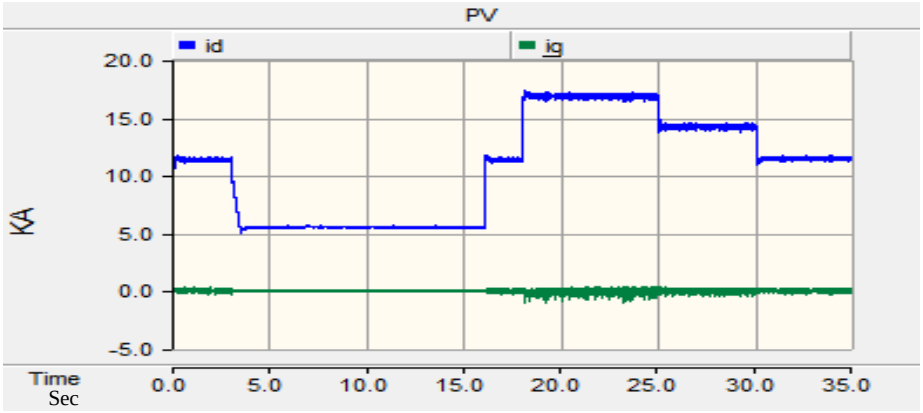

Figure 2.19: *dq*-axis current for one farm.

2.6 Summary

This chapter has successfully modeled and presented a complete study of PV and battery storage penetration. A detailed model of PV with battery storage was built in PSCAD and connected to the isolated northwest grid in Tabuk. That data for that grid were provided by the SEC at the Tabuk branch. In addition, a brief description of the Kingdom's grid was also provided. Different PV power penetration with battery storage were introduced with the THD of the PV current being within the acceptable limit for all penetration stages. Moreover, a unity power factor was achieved by implementing the control scheme described here.

CHAPTER 3

Power Quality Study of an Isolated Northwest Grid of Saudi Arabia with PV and Storage

3.1 Introduction

Power quality, one of the important attributes of a power system, can be disrupted by such disturbance as voltage variation, transient and harmonic distortion, the last one being the most unlikely cause as it is a steady state condition. With the growth of grid connected Photovoltaic (PV), power quality becomes more important because the switching mechanism in the DC-AC inverter can introduce additional harmonics. Moreover, nonlinear loads are becoming widespread due to the use of modern application, resulting in distorted current and voltage in transmission and distribution networks. One approach for addressing this power quality issue is the use of harmonic filters designed to reduce the introduction of harmonic into the network [29].

Appliances such as television, computers, fluorescent lamp and adjustable speed drives (ASD) in air conditioners and heat pumps that uses diode rectifiers to convert AC to DC have a nonlinear characteristic that can introduce harmonics to the current and voltage waveforms. This unwanted phenomena of harmonics can cause additional line losses, damage electrical equipment and interference in communication system. To address these problems requires an analysis of harmonics and nonlinear loads, a common way to analysis and study harmonics is using a linear model to represent a load and then adding nonlinearity by using voltage or current harmonic sources [30].

This chapter includes a study of the power quality for the isolated northwest grid of Saudi Arabia. A detailed PV model with battery storage and various nonlinear loads are discussed as well as the filter design for reducing harmonics distortion.

3.2 Filter Design

Improving the quality of a power system by addressing the harmonics issue can be achieved by various approaches as described in [31]. One frequently used method involves passive shunt filters, which are designed to provide a low impedance path at the tuned frequency to prevent the harmonics current from flowing into the system. The research reported in this chapter used this type of filter since it is the most economical approach for harmonic filtering [29]. One of the most common passive filters is the single tuned filter, which is a capacitor with an impedance of x_c in series with an equal inductance with an impedance of x_L designed to eliminate a certain harmonic so that ($x_c = x_L$) at a tuned frequency (*fn*) [32]. The tuned frequency used in the design of harmonic filters is usually between 2% and 10% below the desired harmonic frequency to avoid parallel resonance and near short circuit at tuned frequency as the filter provides low impedance. Since the dominant component of a passive shunt filter at the fundamental frequency is the capacitor, this filter can be used for power factor correction in order to achieve a desired level.

For a tuned harmonic (h_n) with a capacitor(Q_c), the capactor reacter at *fn* is

$$X_c \cong \frac{KV^2}{Q_c} \qquad (3.1)$$

To eliminate the h_n harmonic, the reactor size should be

$$X_L = \frac{X_c}{h_n^2} \qquad (3.2)$$

The reactance resistor can be calculated as follows

$$R = \frac{h_n X_L}{Q} \qquad (3.3)$$

where Q is the quality factor with a typical value is between 30 and 100 [33].

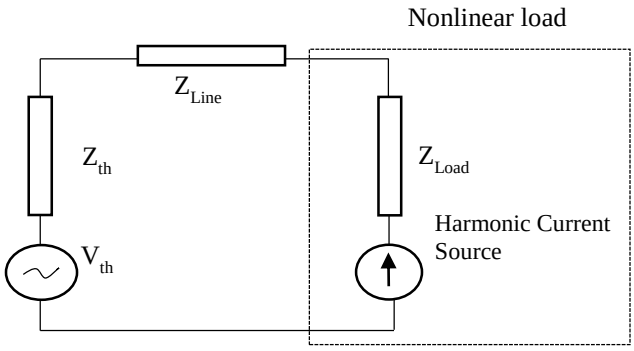

Figure 3.1: Nonlinear load model.

3.3 Nonlinear Load Model

The increase in nonlinear loads due power electronics applications has a significant effect on power system quality, meaning research focused on modeling them and studying their impact on power quality is needed. One common method models a nonlinear load is to model it as a constant impedance at the fundamental frequency component and a current source at the harmonics frequencies [34]. Figure 3.1 shows the equivalent circuit of a power system with a nonlinear load. This chapter explores three of the most common types of nonlinear loads found in residential area, a fluorescent lamp, a computer and an ASD to represent air condition. The percentage of harmonic distortion for each of these nonlinear loads is shown in Table 3.1. By knowing the contribution of each harmonic frequency for a specific load, a harmonic current source can be introduced at each harmonic frequency,

meaning the nonlinear behavior can be modeled by adding the individual harmonic disertion shown in Table 3.1 at each frequency component.

Table 3.1: Harmonic number h(n) VS Individual harmonic distortion [35].

H(n)	***IHD* (%)**		
	Fluorescent lamp	**Computer**	**ASD**
1	100	100	100
2	0.3	3.3	4.12
3	13.9	87.2	0.78
4	0.3	5.1	1.79
5	9	64.1	35.01
6	0.2	1.6	0.215
7	3.3	41.1	2.62
8	0	0	1
9	3.2	17.9	0.06
10	0.1	1.1	0.73
11	0	10.3	9.99
12	0.3	1.2	0.03
13	1.7	10.3	0.19
14	0.3	0	0.48
15	1.9	10.3	0.07
16	0.3	0	0.52
17	0.8	5.1	4.85
THD (%)	18	118.3	37.3

3.4 Simulation Result.

PSCAD software was used to build and simulate the grid with a detailed PV model and battery storage. A peak loading condition for the summer day of July 16, 2013, with a total load of 720 MW was selected for the simulation, and as mentioned in the previous chapter Bus 5 was selected as the slack bus because it has largest capacity. The PV Farm is connected to Bus 6 with a total capacity of 40 MW. The battery is assumed to have a capacity of 50% of the total PV power. A harmonic current source was used to represent

the nonlinear loads, with the harmonic injection based on Table 3.1 being placed at the substation on the low voltage side of 13.8 KV. At each bus the load assumed to be 80 % linear load and 20% nonlinear load. The nonlinear loads used included the ASD representing air condition, the fluorescent lamp and the personal computer with percentage of 18%, 1% and 1% respectively. All loads at each bus reflect a similar assumption. The load at Bus 9 is used here to show the result of including the nonlinear loads. Figure 3.2 illustrates the distorted load current after adding the nonlinear loads. Furthermore, Figure 3.3 shows that the total harmonic distortion (THD) of the load current is above the standard IEEE limit. Thus, a single tuned filter has been designed to eliminate the highest harmonic component, which is the 5th component as shown in Figure 3.4. Figure 3.5 shows the load current after installing the 5^{th} harmonic filter, and Figures 3.6 to 3.11 provides the THD for each bus. It can be seen in Table 3.2 that the distortion falls to within the limits based on the IEEE standard [36].

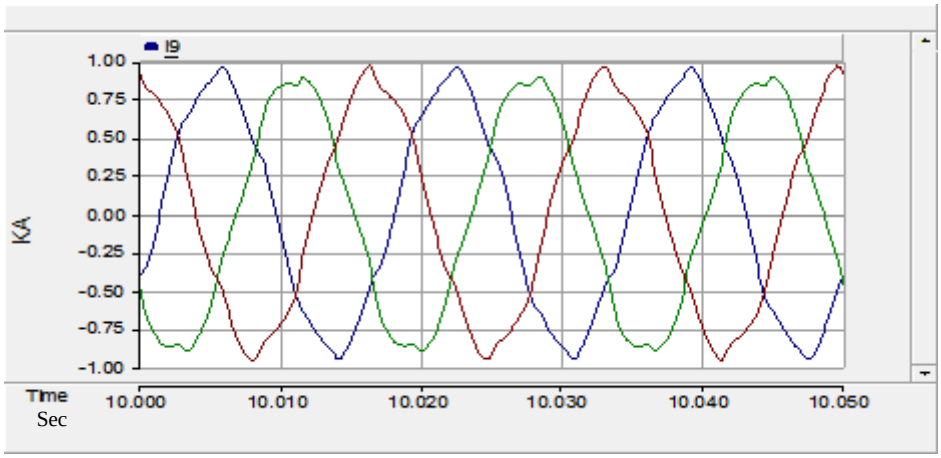

Figure 3.2: Load current without filter of Bus 9.

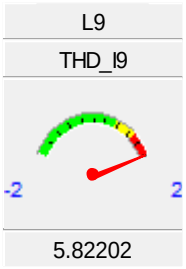

Figure 3.3: THD at Bus 9.

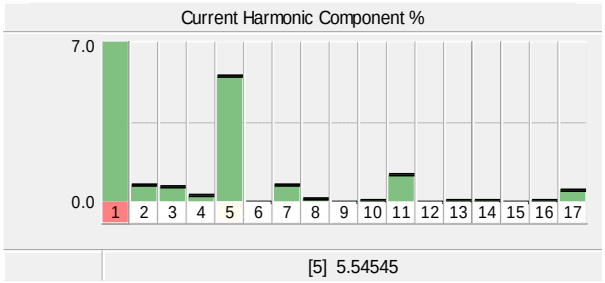

Figure 3.4: Harmonic component.

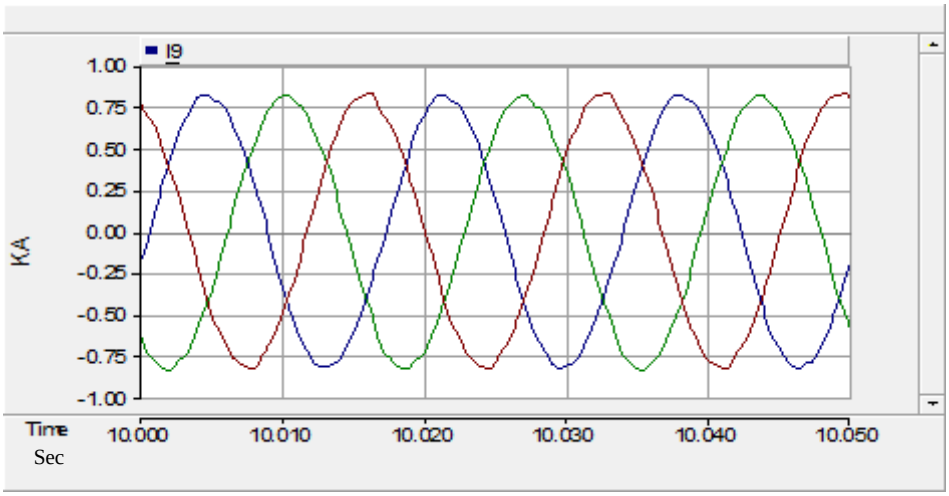

Figure 3.5: Load current with filter of Bus 9.

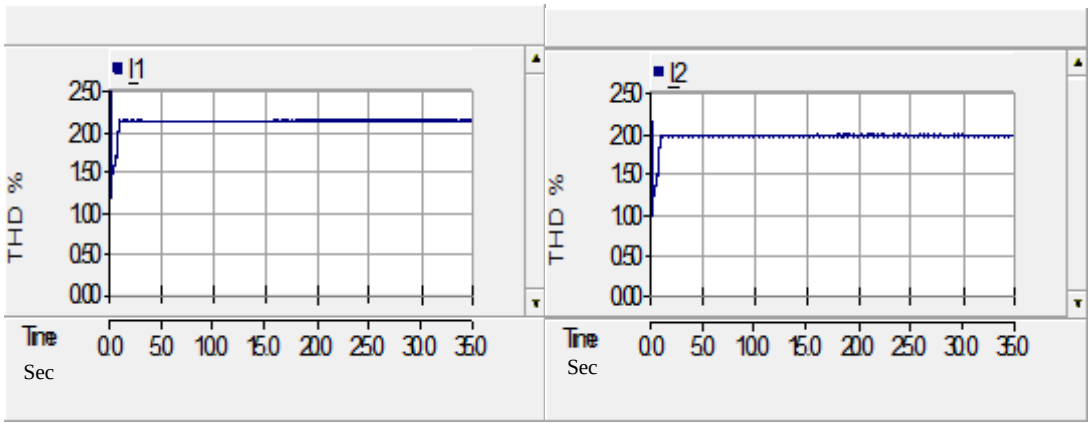

Figure 3.6: THD of load current at Buses 1 and 2.

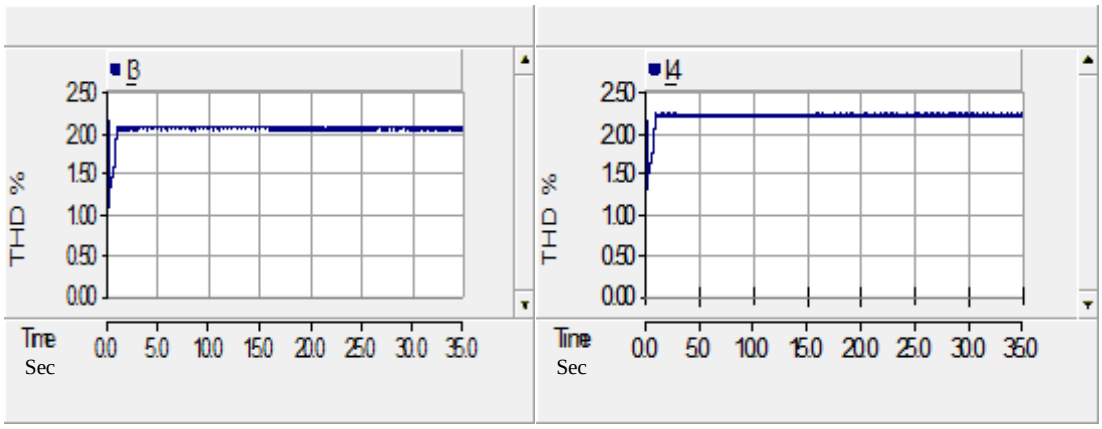

Figure 3.7: THD of load current at Buses 3 and 4.

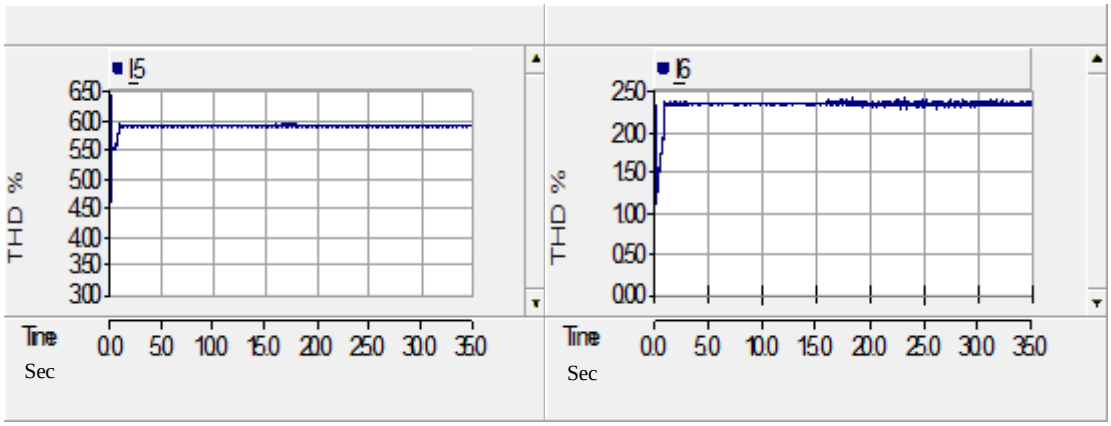

Figure 3.8: THD of load current at Buses 5 and 6.

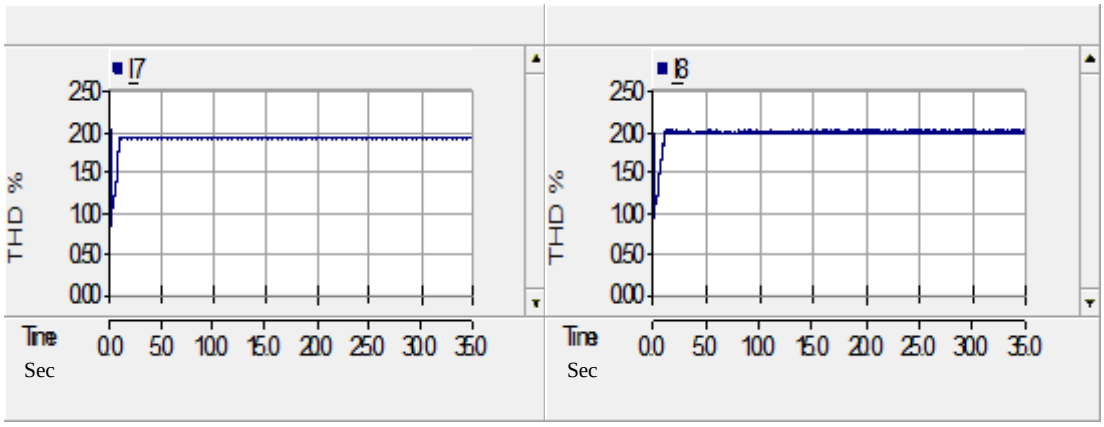

Figure 3.9: THD of load current at Buses 7 and 8.

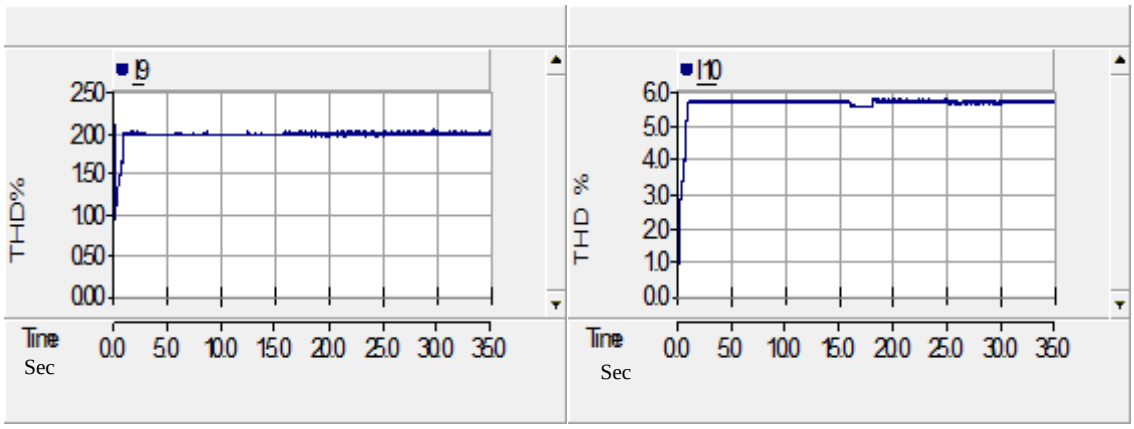

Figure 3.10: THD of load current at Buses 9 and 10.

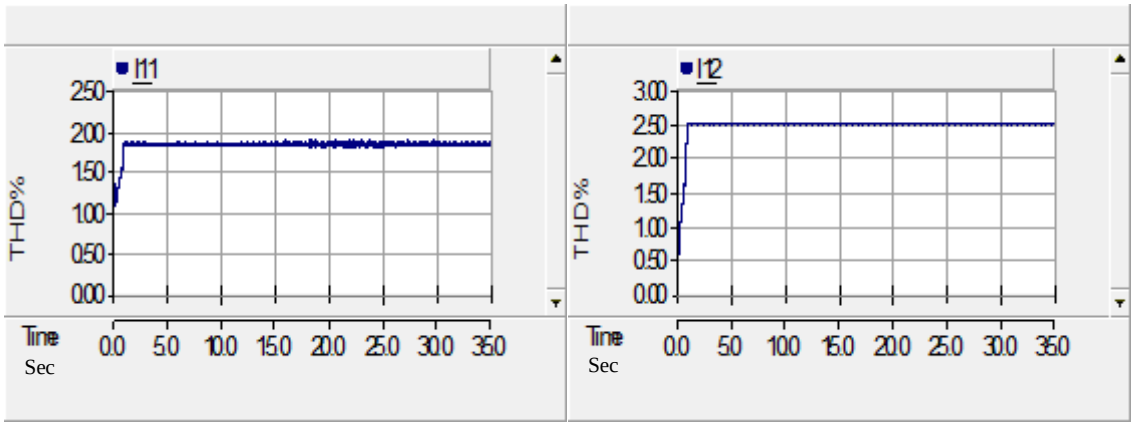

Figure 3.11: THD of load current at Buses 11 and 12.

Table 3.2: THD of load current compared with the standard Limits.

Bus No.	1	2	3	4	5	6	7	8	9	10	11	12
THD% for load Current	2.11	1.96	2.03	2.18	5.87	2.33	1.90	1.97	1.98	5.63	1.83	2.49
$\frac{I_{sc}}{I_L}$	<20	<20	<20	<20	50<100	20<50	<20	<20	<20	50<100	<20	<20
IEEE Limit % for 132 KV level	2.5%	2.5%	2.5%	2.5%	6%	4%	2.5%	2.5%	2.5%	6%	2.5%	2.5%

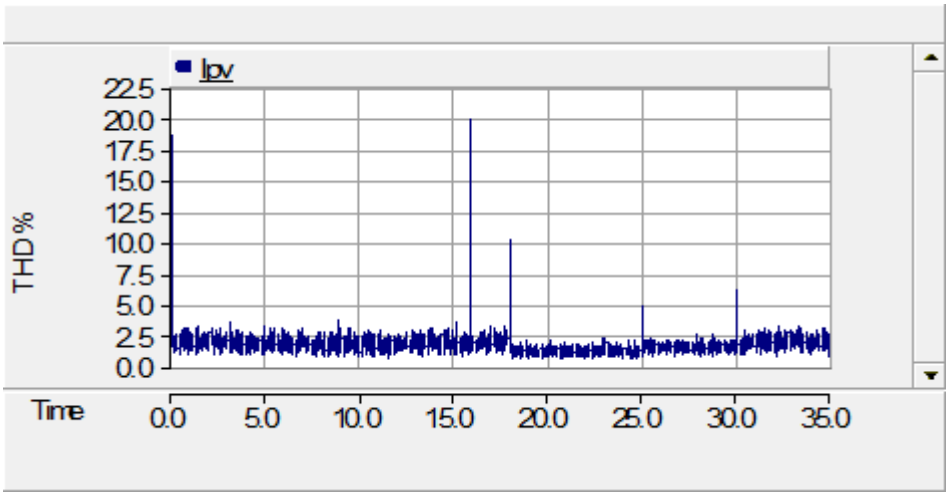

Figure 3.12: THD of PV current at PCC.

The THD of the PV current injected into the grid for all different penetrations is within the acceptable limits. It is oscillating around 2.5% as seen in Figure 3.12, whereas it fluctuates around 2% without modeling the nonlinear load as shown in Figure 2.17. This increase, although within acceptable limits, is due the introduction of the harmonics from other buses which remain even after the filter was installed.

3.5 Summary

This chapter presents a power quality study for the northwest grid of Saudi Arabia with a PV and battery storage. Various PV power penetrations with battery storage were introduced, and the THD of the PV current was found to be within the acceptable limits for all penetration levels. In addition, nonlinear loads were included for further analysis, the results showing that the harmonic impact of introducing such loads was solved by introducing passive filters.

CHAPTER 4

Optimal Operation of a Power System

4.1 Introduction

The rapid development of such sectors such as industry, transportation and communication highlights the necessity of a sufficient supply of electrical energy. This emphasizes its important as a basic factor in the modern economy, one that has led to an increase in the number of power stations, generation capacities, and electricity networks. Thus, the economic operation of a power system has become a high priority, one that can be achieved by Economic Dispatch (ED): finding the best generation schedule to satisfy the required demand and the constraints of the system with minimum production cost [37].

In the past, various mathematical programming and optimization techniques, such as the Lambda iteration method [38], the gradient method [39] and the Newton method [38], have been applied to ED problems. However, the assumption of the incremental costs of a generator cannot be accurately represented as an increasing function due to the nonlinear characteristic of the thermal unit. As a result, dynamic and nonlinear programming techniques have been suggested in the literature for solving ED problems [40, 41], with ED more appropriately belonging to the latter category due to the nonlinearity characteristic of the power system and thermal units [42]. One of the effective techniques for finding global minimum for optimization problems with quadratic objective and linear constraints is quadratic programming [43]. This study applies the optimization method of mixed integer quadratic programming (MIQP) since the generation cost curve is a quadratic function [44].

This chapter discusses the classical ED and the MIQP technique for solving optimization problems

4.2 Classical Economic Dispatch

In the context of a power system, the purpose of ED is to find the output power of the generators needed to meet the load demand while at the same time minimizing the operation cost under various operating conditions and system constraints

4.2.1 Input-Output Characteristic of Thermal Unit

ED can best be described as an approach for supplying and delivering the power from the unit that has the highest efficiency at the minimum cost. As the load increases, the unit will continue supplying the power to the system until maximum efficiency is reached. If further the load is needed, the second most efficient unit will begin to deliver power to the system, with the third unit commencing operation once the second one reaches its maximum efficiency. However, even without considering transmission lines losses, this strategy does not result in minimum operational cost.

The economical distribution among all generators can be measured through the operation cost in terms of power output, with fuel cost being the key factor for fossil fuel units. The input-output characteristic curve of a thermal unit reflects the relationship between fuel consumption and the output power, which is referred to as the operational cost function. Figure 4.1 shows a typical plot for the input-output curve of a thermal unit, representing the relationship between the fuel inputs in British thermal units per hour

(Btu/h) versus the power output in megawatts (MW). By multiplying the fuel input by the fuel cost, the curve is converted to dollars per hour ($/h) versus power [44-46].

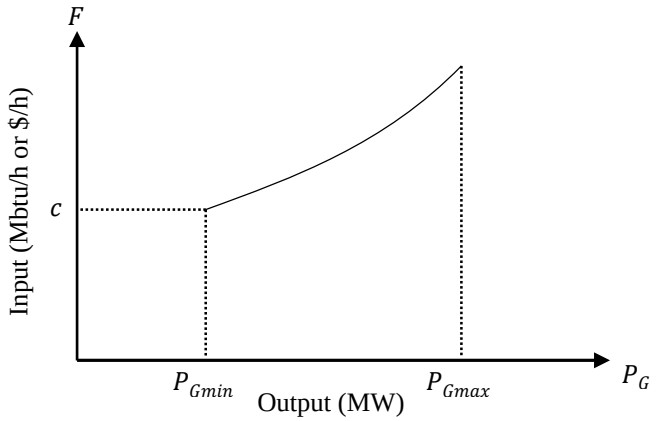

Figure 4.1: Input output characteristic curve of a thermal unit.

Additional operation costs such as labor and transportation are considered to be constant because of the difficultly involved in defining them as a function of cost.

The output power of a generator is bounded between the minimum and maximum capacity depending on the manufactures' design of the thermal unit. In general, the input-output characteristic curve of a thermal unit has a nonlinear relationship, which is usually defined as a quadratic function as seen in Equation 4.1 below:

$$F = a + bP + cP^2 \quad (\$/h) \qquad (4.1)$$

where a, b and c are coefficients for the characteristic curve and a is the fuel consumption of the unit without power output. These coefficients can be determined using the methods listed below [47]:

1- Experimenting with the unit efficiency.

2- Using the historical record of the unit.

3- Using the manufactures' data design.

4.2.2 ED Problem Formulation

As the primary goal of ED is to supply the demand (P_{Demand}) at minimum operation costs and losses with respect to various constraints [48, 49], ED is a constrained optimization problem with the following objective function:

$$\min = \sum_{i=1}^{N} F_i(P_{Gi}) \quad (4.2)$$

where

$$F_i = a_i + b_i P_{Gi} + c_i P_{Gi}^2 \quad (4.3)$$

N represents the total number of generators in the system; P_{Gi} the output power of the i^{th} generator; $a_i, b_i and\ c_i$ the i^{th} generator's coefficient; F_i the cost in dollars per hour of the i^{th} generator. This optimization problem is subjected to the following constraints:

1- Equality constraints as expressed in the power balance equations:

$$\sum_{i=1}^{N} P_{Gi} - P_{Demand} - P_{loss} = 0 \quad (4.4)$$

$$P_{loss} = \sum_{i=1}^{N} \sum_{j=1}^{N} P_{ij} + B_{ij} P_j + \sum_{i=1}^{N} B_{0i} P_i + B_{00} \quad (4.5)$$

where B_{ij} is the loss coefficients described in [44].

2- Inequality constraints

The output power of a generator should operate within the range between its maximum and minimum capacity

$$P_{iG\ min} \leq P_{Gi} \leq P_{Gi\ max} \quad (4.6)$$

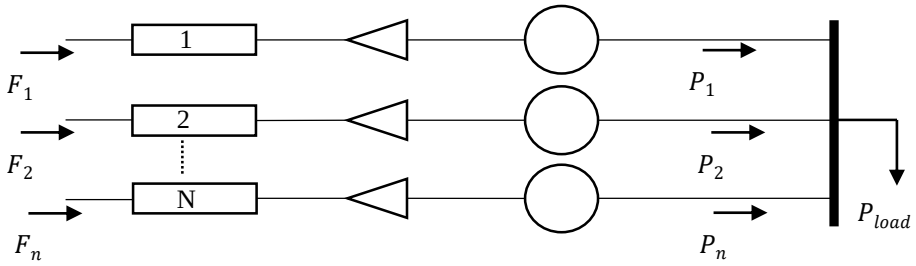

Figure 4.2: N thermal units supplying a load [48].

4.3 Optimization Methods

Optimization searches for the best possible solution for a problem having a number of competing or conflicting constraints. The methods for performing this search can be categorized into the three approaches listed below [50]:

- Conventional optimization approaches including unconstrained optimization methods such as the Newton-Raphson Method, the Gradient Descent Method, Quadratic Programming (QP), Linear Programming (LP), and Nonlinear Programming.

- Artificial Intelligence techniques such as Neural Network (NN), Evolutionary Algorithms (EAs), Tabu Search(TS), Particle Swarm Optimization (PSO), Ant colony, and Simulated annealing.

- Non-equality approaches that address uncertainties in objectives and constraints, including Fuzzy set applications, Probabilistic optimization, Analytic Hierarchical Process (AHP).

4.4 Mixed Integer Quadratic Programming (MIQP)

MIQP is considered a special condition of Mixed Integer Nonlinear Programming (MINLP). Its fundamental principle appears to be identical to the normal quadratic programing problem. However, the former includes an important feature: the optimization variables combine both real and integer values. A special situation of MIQP, referred to as Mixed Binary Quadratic Programing (MBQP), which also defined as MIQP in literature [50], involves constraining the integer variables to binary numbers 0 or 1. While various methods and techniques can be used to solve MIQP problems, the common approaches include [51]:

1. Branch and bound methods.
2. Decomposition methods.
3. Cutting plane methods.
4. Logic-based methods.

Of these, the branch and bound method is believed by most researchers to be the most effective approach for solving MIQPs [51]. There are several software programs for solving MIQP problems, One of the most common being CPLEX.

4.4.1 Problem definition

MIQP is defined as follows:

$$\min_{x} \frac{1}{2} x^T H\, x + f^T x \qquad (4.7)$$

subjected to

$$A_{eq} x = b_{eq}$$

$$Ax \leq b$$

$$l_b \leq x \leq u_b$$

$$x_i \in Z$$

$$x_j \in \{0,1\}$$

where H is a $(n\ x\ n)$ sparse matrix representing the quadratic term [52]. The linear term f is an $(n\ x\ 1)$ vector included in the quadratic objective function subjected to the following constraints:

1- Linear inequalities

   A is an $(m\ x\ n)$ matrix representing the linear coefficients, and b is an $(m\ x\ 1)$ vector representing the constant vector.

2- Linear equality

   A_{eq} is a $(k\ x\ n)$ matrix representing the linear coefficients, and b_{eq} is a $(k\ x\ 1)$ vector representing the constant vector.

3- Decision variable bounds

   l_b and u_b are $(n\ x\ 1)$ vectors representing lower and upper bound, respectively.

4- Integer constraints

   x_i is a composed of decision variables that must be an integer.

5- Binary constraints

x_j is a composed of decision variables that must be a binary numbers (0,1), $i \neq j$.

The aim of such optimization is to minimize the objective function by choosing a value of x that satisfies all constraints.

4.4.2 Branch and Bound

Disregarding the computational burden, for any optimization problem that includes binary variables, the simplest approach for gaining optimality first lists all the potential combinations of the binary variables and then calculates the optimal solution individually for any involvement of real variables in the optimization. Next, the optimal solution is selected by comparing all solutions based on the best objective function. The total number of binary variables combinations is 2^{nb} , where nb is the number of binary variables, with the computational load of the problem becoming larger as the binary variable increases [50]. For this reason, it is essential to find an algorithm that is able to compute the optimal solution without considering all potential binary variable combinations [50]. One algorithm, the branch and bound method, meets this requirement as it considers only selected scenarios of possible combinations. More details about its derivation and motivation is found in [53, 54]. Figure 4.3 shows the possible combinations of two binary variables represented by what is referred to as binary search tree.

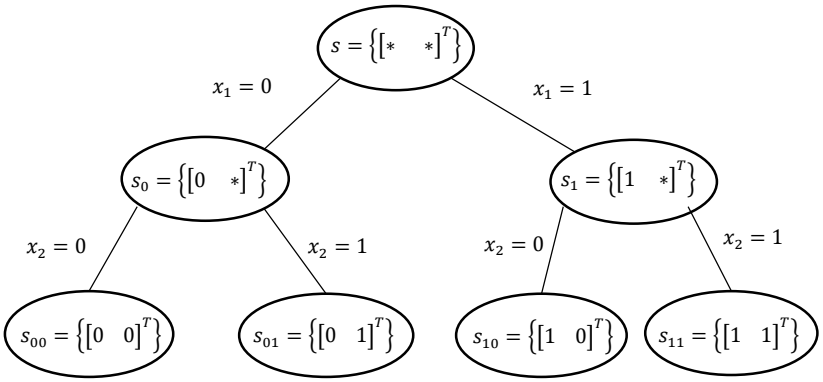

Figure 4.3: Binary search tree [50].

where x_1 and x_2 represents two binary variables, S_i a feasible set, and * Variable is free to be 0 or 1.

As the structure seen in Figure 4.3 shows, the optimization problem is actually composed of subproblems represented by the subtree. One of the primary ways to address the computation burden is to find the lower and upper bounds of the objective function for the subproblems in the nodes as theses bounds can be used to remove the entire subtrees, which subtrees are then no longer considered in the optimization process because none include the best solution. Furthermore, it is easier to compute those bounds than solve the original problem to optimality. Figure 4.4 illustrations an example of using such bounds for solving and minimizing the original problem over set *S*. This problem is composed of two subproblems: the first one involves setting the binary variable x_1 to 0 and the second sets it to 1. As can be seen in Figure 4.4, the best possible objective function value over S_1 (S_1 = 6) is higher than the worst possible solution over S_0 (S_0= 5), denoting that the optimal solution is not found in S_1. Hence, this root node can be removed. Applying this technique requires a method for finding the upper and lower bounds. Generally, upper bounds can be

obtained from the integer feasible solution, while the lower bounds can be obtained from relaxations. In MIQP, the integer constraints are relaxed to interval constraints [50].

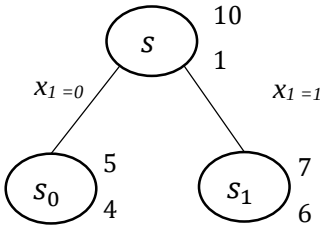

Figure 4.4: Shows an example of using bounds to eliminate nodes [50].

4.5 Test System

This optimization approach based on MIQP with a branch and bound algorithm was applied to the isolated northwest grid in Tabuk city consisting of 12 buses as shown in Figure 2.11, with a voltage level of 132 KV. It includes two generation stations, connected at Buses 1 and 5, consisting of 25 units with total capacity of 959.2 MW. The generation capacity and age of each unit are shown in Table 4.1. A standard IEEE fuel cost curve and a fixed startup cost were used for the newest unit, while the cost curves of the remaining generators have been modeled based on the unit's age by decreasing the efficiency of the standard one, meaning that newer generators have lower fuel cost than the older ones. Since the age of each unit is based on 2013, a load curve for a summer day in July of that year was used for the simulation, with the load profile and lines data being provided by the Saudi Electricity Company (SEC), Tabuk sector.

4.6 Problem Formulation

In this chapter, only conventional generators without renewable resources were considered in the optimization process. In addition, the startup cost was also included, but the power losses were not.

4.6.1 Power Balance Equation

For the power balance equation, Equation (4.8) below, the algebraic sum of the power generated by the generators should be equal to the power demand for all dispatches:

$$\sum_{i=1}^{nGen} P_i(t) - P_{LD}(t) = 0 \quad \forall t \in T \tag{4.8}$$

4.6.2 Generation Limits

The amount of power generated and the ramp up/down rate for each generator are constrained as follows:

$$\underline{P_i^g} \leq P_i^g(t) \leq \overline{P_i^g} \tag{4.9}$$

$$\underline{\Delta P_i^g} \leq \Delta P_i^g(t) \leq \overline{\Delta P_i^g} \tag{4.10}$$

4.6.3 Fixed Cost for the Generator

The fixed cost for the generator was model as seen in Equation (4.11), where β is a binary variable. Hence, whenever non-zero power is produced by the ith generator, β_i is be 1 and 0 otherwise.

$$\beta_i(t) \,.\, \overline{P_i^g} \geq P_i^g(t) \tag{4.11}$$

4.6.4 Startup Cost

Equation (4.12) ensures that γ is 1 whenever a unit is coming online after being off in the previous dispatch.

$$\gamma_i(t) \geq \beta_i(t) - \beta_i(t-1) \tag{4.12}$$

4.6.5 Objective Function

The objective function for this simulation is given below

$$\min \sum_{i=1}^{N} (\beta_i(t).a_i + b_i P_i^g(t) + c_i P_i^g(t)^2).\Delta t + \gamma_i(t).C_{i,str}^g \quad \forall t \in T \tag{4.13}$$

where $a_i, b_i \; and \; c_i,$ represent the fuel cost coefficient of generator i, $C_{i,str}^g$ represents the startup cost of generator i , and Δt is the dispatch interval.

4.7 Simulation Result

The summer load curve was selected for the simulation based on Figure 2.12 in chapter 2. On that day in July, the generated power at peak load occurred at 4 pm with a total load of 720 MW. The dispatch interval was set for every 15 minutes with a specified ramp up/down of 2 MW/min. The model was implemented in MATLAB using CPLEX [55] to solve the MIQP. The performance of the optimization problem can be measured by the integrality gap, defined as the gap between the optimal value of the relaxed solution and the optimal integer solution [56, 57].

Table 4.1: Shows all generators (diesel) capacity [58].

Station	Unite No.	Unit Age	Unit Capacity	Efficiency
Tabuk-1 (102 MW)	1	34	5.7	65% to 60%
	2	34	5.7	
	3	34	5.7	
	4	34	5.7	
	5	34	5.7	
	6	34	5.7	
	7	32	17.1	
	8	31	17.1	
	9	30	16.8	
	10	30	16.8	
Tabuk-2 (857.2 MW)	11	27	27	82% to 68%
	12	27	27	
	13	22	31.2	
	14	16	57.7	
	15	16	57.7	
	16	13	60.1	
	17	8	61	95% to 87%
	18	7	61	
	19	4	65.5	
	20	4	65.5	
	21	4	65.5	
	22	1	78	
	23	1	78	
	24	0	61	
	25	0	61	

Table 4.2: Standard IEEE coefficient for the fuel cost curve [59].

Fuel Cost Coefficients	
a_i (\$)	287.4982
b_i (\$/MWh)	19.7128
C_i (\$/MWh^2)	0.0224
Startup cost \$	1511.899

Table 4.3: shows the optimal operation cost for Tabuk grid.

Case	No. of generators removed	Best Integer Solution ($)	Time (S)	Gap	Penetration	
					Tabuk-1	Tabuk-2
A	None	402190	7.5	0.02%	No	Yes
B	One large	411260	4.1	0.05%	No	Yes
C	Two large	429380	1.8	0.00%	Yes	Yes
D	Three large	456660	60	1.00%	Yes	Yes

Table 4.3 shows the optimal solution of one minute simulation for different cases. The cases are defined by removing up to 3 large generators due to maintenance from Tabuk-2, which has the most new generators and the largest capacity. As seen in Case A, when all generators are available, only Tabuk-2 is operating. When scheduling one generator for maintenance, Tabuk-2 can continue supplying the required demand as seen in Case B. However, when scheduling two and three generators for maintenance as shown in Cases C and D, respectively, Tabuk-2 is able to meet the demand during normal operation at optimal operational cost, but Tabuk-1 operates to compensate for the lake of power during peak times as seen in Figures 4.5 and 4.6, meaning Tabuk-1 is needed only in emergency situations, important since it is an old station with low efficiency.

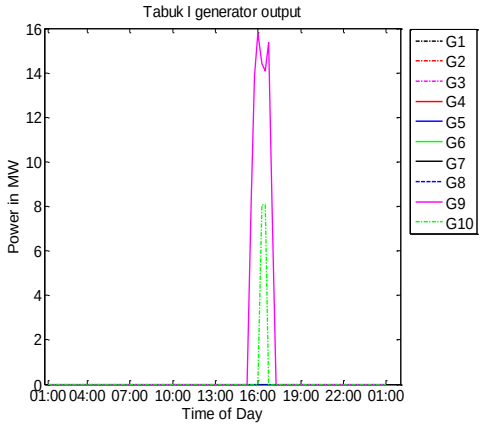

(a) Scheduled power for Tabuk-1

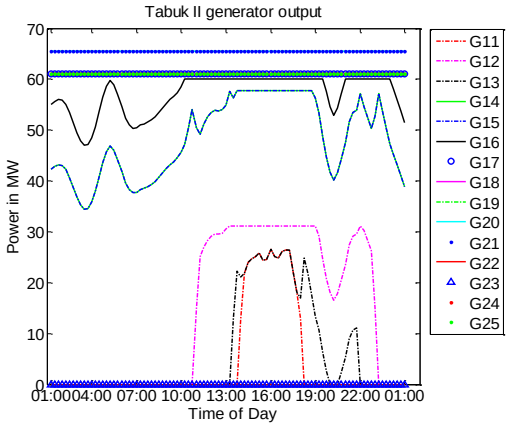

(b) Scheduled power for Tabuk-2

Figure 4.5: Scheduled power for Case C: (a) Tabuk-1 generators output, (b) Tabuk-2 generators output.

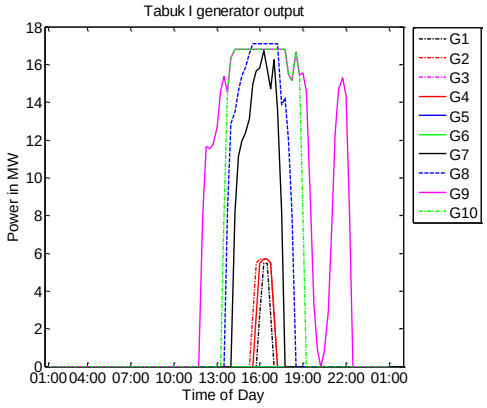

(a) Scheduled power for Tabuk-1

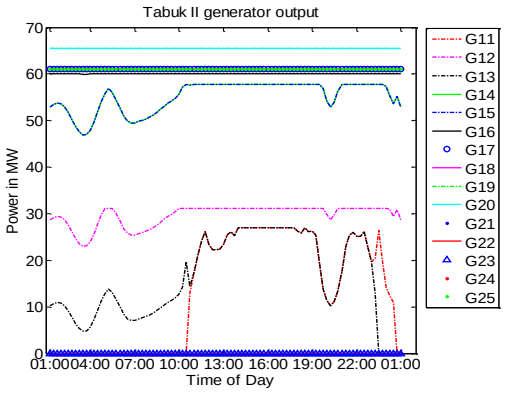

(b) Scheduled power for Tabuk-2

Figure 4.6: Scheduled power for Case D: (a) Tabuk-1 generators output, (b) Tabuk-2 generators output.

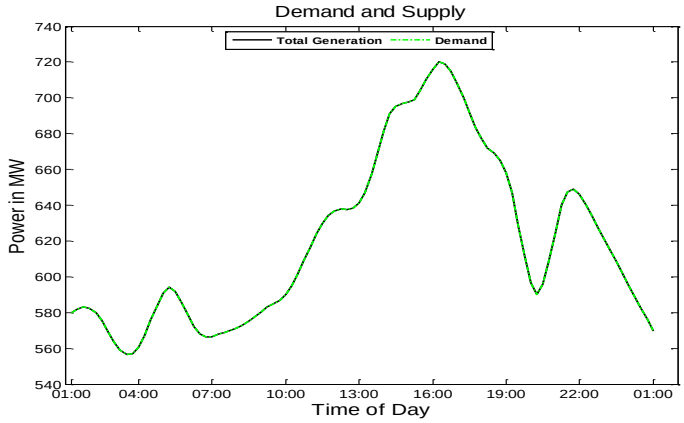

Figure 4.7: Supply and demand.

4.8 Summary

Economic operation, a major requirement for power system, can be achieved through economic dispatch. This chapter introduced several options for minimizing operation cost while still meeting the load demand and all of the constraints, analyzing the classical method of ED and introducing various optimization techniques. It then explored MIQO and its problem formulation, applying this optimization method to the isolated grid in Tabuk city. This research then reduced the computation burden for the optimization problem using the branch and bound approach. The simulation results indicate that Tabuk-2 can supply the required demand at optimal operational cost; however, during an emergence such as generator being off due maintenance scheduling or faulty equipment, Tabuk-1 is needed to help supply demand during peak times.

CHAPTER 5

Secure Operation and Optimal Generation Scheduling Considering Battery Life

5.1 Introduction

Maintenance schedule of generators in an interconnected power system presents multifaceted challenges, two important ones being optimal operation cost and secure operation. When a generator is scheduled for maintenance, achieving optimal generation scheduling for the committed generators is necessary but it is not sufficient for secure operation of power systems. This problem is decomposed into two subproblems: i) Finding the optimal set points for the generators ii) Validating secure operation with those set points from (i). Both these subproblems (i and ii) have been studied extensively in the literatures. However, the research here focuses on incorporating battery energy storage systems (BESS) in power opreation, a renewable generation that can provide a smooth and flexible reserves of power, an area that has not yet been fully explored. In addition, incorporating BESS while considering both the cost implications and addressing secure operation has not yet been addressed in previous literatures. The purpose of this chapter is to present a detailed mathematical model to address this issues.

With increasing load demand, renewable generation has provided a viable means for reducing emissions and operational costs. In particular, the use of solar generation has seen a significant increase over the last decade. However, the random power output of PV has created several challenges in power system operation and control. Renewable generation is categorized as non-load following generation as its output cannot be controlled. The inter-dispatch variability of renewable generation that is geographically distributed, to a

large extent, is smooth. However, scenarios such as the one considered in this work where the renewable generators are not geographically distributed present a considerable challenge with respect to variability and availability [60]. One of the solutions potentially addressing the challenge of solar variability is to use battery storage, which has been found to be particularly effective when working in parallel with PV in peak load shaving as presented in [61, 62]. Renewable energy systems today are sufficiently developed and are widely used to address environmental and economic dispatch (ED) concerns. Storing energy at off-peak times when there is additional generation capacity and then using this stored energy will make the economic dispatch (ED) more efficient in terms of operating cost. Time shifting renewable energy generation through the use of BESS will help reduce the operating cost in this scenario as the incremental cost of producing power through controllable generation is lower at certain levels of loading [63].

Many studies have been introduced for optimal operation with PV and battery storage. For example, the Authors in [64] presented an optimal battery scheduling plan with emission constrains to reduce the carbon footprint of conventional thermal units. Reference [65] proposed an optimal peak shaving by managing energy storage devices, and the research presented in references [66, 67] proposed optimal charging/discharging scheduling of BESS to minimize line losses in distribution systems. In [68] an optimal power management for grid connected PV system with batteries is proposed to minimize customer energy bills, and an optimal scheduling of battery storage presented in [59] is used to evaluate the optimal amount of installed battery into the grid by considering the CO_2 emission in the economic evaluation. The authors in [69] proposed an optimal

scheduling of non-utility facility with battery storage under a price taking scheme. None of these studies, however, considered the battery life in the cost function. Disregarding the battery life in optimal power scheduling is an unrealistic scenario. Although BESS lowers operating costs, the life of the battery is significantly reduced. As BESS require substantial investment, it is imperative that they be used effectively and efficiently such that the economic and security margins of the power grid operation are maximized.

This chapter presents an optimal generation scheduling taking onto consideration renewable energy sources, BESS usage cost, and secure operation. In addition, it also proposes an optimal generation schedule considering battery life and short term outages: resulting in extended battery life and finding a solution during outages without affecting the optimal operation. Feasibility of this proposed approach is demonstrated using Tabuk power system – an isolated northwest grid of Saudi Arabia.

5.2 PV Output Power

The summer irradiation data for Tabuk city used here was taken from Renewable Resource Atlas of Saudi Arabia [70]. The station data is located at Tabuk University, at Latitude of 28.38287 (N) and Longitude of 36.48396 (E). Figure 5.1 shows the irradiation profile for 31 August 2015. To simulate the PV output power of the farm, the Wavelet Variability Model Toolbox in Matlab was used; the details and validation of this model are described in [71, 72]. In this chapter, a 100 MW solar PV farm is simulated to be included in the optimization process. Figure 5.2 illustrates the PV power for the solar farm.

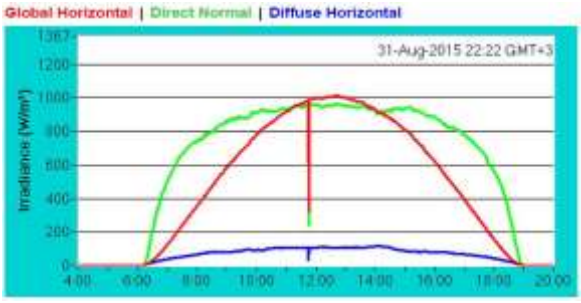

Figure 5.1: Irradiation data.

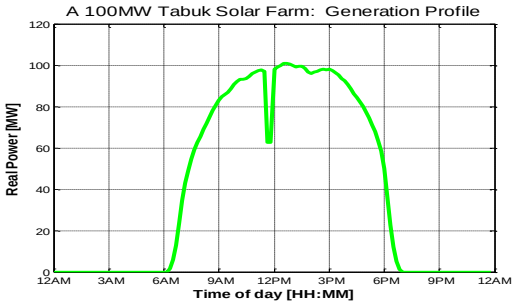

Figure 5.2: PV output power.

5.3 Battery Usage Cost

The levelized cost of the battery is adopted in defining the usage cost to quantify the charge/discharge cycle in the optimization process. Thus, the formulation explicitly involves the life cycle of the BESS based on the definition of a usage cost as given in Equation (5.1), which imposes the physical degradation of the BESS. Excluding the life cycle creates unrealistic situation and exaggerates the significance of BESS on system operation at minimum cost. The cost of the battery is not estimated; rather it is specified based on the battery markets and prices for large scale storage. The goal here is to achieve minimum operational cost while at the same time extend the life of the battery by using it only when needed.

The levelized cost of energy (LCOE), which provides a more accurate reflection of the actual cost of a given battery, helps to determine the cost ($/kwh) involved in charging and discharging the battery over its lifetime. This cost is used as the usage cost for the battery. The LCOE is calculated as follows [73];

$$LCOE = \frac{Cost}{Energy\ Capacity \times cycles \times round\ trip\ efficincy} \tag{5.1}$$

The cost in Equation (5.1) includes installation costs, variable and fixed operation and maintenance costs. Moreover, the battery replacement cost is also involved since the battery will be replaced once, at the year 8 of a 15-years period. A lead acid battery is used and the battery data with its cost are based on the battery markets and prices [74]. Table 5.1 shows the battery parameters and cost.

Table 5.1: Battery data and cost [74].

Battery Cost and Data	
System capacity- kw	50,000
Depth of discharge (DOD)per cycle %	80%
Energy capacity- kwh @ rated DOD	250,000
Round trip Efficiency- %	85%
Number of cycle per year	365
Plant life, years	15
$/ kwh @ rated DOD	$349
Fixed O&M - $/kw-year	$4.5
Variable O&M - $/ kwh	$0.0005
Battery replacement- years	8
Replacement battery cost - $/kw	$337

Thus,

$$LCOE = \frac{250{,}000 \times 349 + 250{,}000 \times 0.0005 + 50{,}000 \times 4.5 \times 15 + 337 * 50{,}000}{250{,}000 \times 365 \times 15 \times 85\%} = 0.09237\ \$/kwh$$

5.4 Problem Formulation

Many methods have been used by the power industry to solve economic dispatch problems in order to minimize the operation cost. The complexity of the problem and the economic benefit gained from cost minimization have motivated both the academia and the industry to develop improved optimization techniques [75], resulting in shuch promising methods such as Lagrangian Relaxation, Dynamic Programming, Branch and Bound Mixed Integer Programming and Bender Decomposition Methods [76-78]. Recent developments in integer programming propose additional promising methods to acquire improved solutions for large scale systems more rapidly [75]. In this work, the fuel cost curve is approximated using a quadratic function. Hence, the ensuring formulation is of mixed integer quadratic programming (MIQP) type.

5.4.1 Energy Storage

Equation (5.2) below is the energy balance equation the (BESS) [79], while Equations (5.3)-(5.5) give the bounds for the rate of charge and discharge and the battery storage limits.

$$E(t) = E(t-1) + P^{C}(t)\,.\,\eta_{in}\,.\,\Delta t - \frac{P^{D}(t)}{\eta_{out}}\,.\,\Delta t \qquad (5.2)$$

$$0 \leq P^{C}(t) \leq \overline{P_B} \qquad (5.3)$$

$$0 \leq P^{D}(t) \leq \overline{P_B} \qquad (5.4)$$

$$\underline{E} \leq E(t) \leq \overline{E} \qquad (5.5)$$

Equation (5.2) is of particular importance because $P_i^C(t)$ and $P_i^D(t)$ are free variables that could take non-zero values in any dispatch. However, in reality the BESS can either

charge or discharge during a given interval but not both. This condition is enforced with the use of a binary variable such as

$$\alpha \,.\, \overline{P_B} \geq \; P^C(t) \tag{5.6}$$

$$(1-\alpha) \,.\, \overline{P_B} \geq \; P^D(t) \tag{5.7}$$

Although Equations (5.6) and (5.7) ensure that only charging or discharging occurs during a given dispatch, such a modeling requires the use of the binary variable α, increasing the computation effort required to solve the problem. Instead, the need for binary variables is avoided because of their implicit inclusion in the objective function. AS Charging and discharging in the same dispatch result in an inefficient use of the energy and, hence, would increase the total cost, the optimizer would never charge and discharge at the same dispatch and instead schedules charging and discharging in an optimal manner.

5.4.2 Power Balance Equation

Equation (5.8) is the power balance equation. The algebraic sum of the power generated by generators, the PV power and the BESS should equal to the power demand for all dispatches.

$$\sum_{i=1}^{nGen} P_i(t) + P_{pv}(t) + P^D(t) - P^C(t) - P_{LD}(t) = 0 \quad \forall t \in T \tag{5.8}$$

5.4.3 Generation Limits

The amount of power generated and the ramp up/down rate for each generator are constrained by Equations (4.9) and (4.10) as shown in the previous chapter.

5.4.4 Fixed Cost for the Generator

The fixed cost of the generator is modeled as presented using Equation (4.11).

5.4.5 Startup Cost

The startup cost is constrained by Equation (4.12).

5.4.6 Objective Function

The cost function, defined as the fuel cost of all generators, the startup cost and the battery usage cost, is formulated as follows:

$$min \sum_{i=1}^{nGen} \left\{ \left(\beta_i(t).a_i + b_i.P_i^g(t) + c_i.P_i^g(t)^2 + C_B.(P^C(t) + P^D(t)) \right).\Delta t + \gamma_i(t).C_{i,str}^g \right\} \ \forall t \in T \quad (5.9)$$

where $a_i, b_i \ and \ c_i,$ represent the fuel cost coefficient of generator i, $C_{i,str}^g$ the startup cost of generator i , Δt the dispatch interval and C_B the battery usage cost computed based on the LCOE.

5.5 Forced Contingency Analysis

Forced contingency can be described as any outage of a grid component such as a line or a transformer and/or a generator due to a fault. These outages can cause voltage or line limit violations due to the resulting overloading. A contingency, thus, is defined as a possibly harmful disturbance that may occur during operation. However, in normal operation conditions, contingency analysis is used under heavily loaded systems to provide a list of lines to be ranked in order to help relieve the overloading of the system by removing a line (N-1). If one line does not relieve the overload, then another line is removed (N-1-1).

This research focused in forced contingency during optimal operation to provide the operators with an overview of the system and a solution for any of the outages in order to maintaining optimal operation. Hence, different cases will be applied to the system. For

each case, the optimal operation cost is obtained, followed by a line outage due to a fault. An improved solution for any outage may be provided by removing another line to ensure optimal operation is maintained without any violations.

5.6 Simulation Result

From the recorded data obtained for the summer day used in this study, the peak loading condition was used as the worst case scenario for the test system. On that day, the generated power at peak load occurred at 4 pm with a total load of 720 MW. The battery storage constraints used in the simulation shown in Table 5.2 are based on the battery data given in Table 5.1. The dispatch interval was every 15 minutes, with a specified ramp up/down of 2 MW/min. The model was implemented in MATLAB using CPLEX to solve MIQP. The performance of the optimization problem can be measured by the integrality gap, defined as the gap between the optimal value of the relaxed solution and the optimal integer solution.

Different situation were applied to the system, with optimal operation cost being obtained for each. In addition, forced contingency analysis was implemented by tripping a line due to a fault. When such a violation occurred, a search of a solution for any overloaded lines was obtained. Violation were addressed by removing another line to maintain the stability of the system. Similarly, the cases can be extended to generators/transformers maintenance scheduling, with such cases involving removing one or more generators from Tabuk-2. The specified cases investigated in this research include the follows:

1. Case A: All generators in Tabuk-2 are ON, full capacity 959.2 Mw.

2. Case B: One large generator in Tabuk-2 is removed, remaining capacity 881.2 Mw.
3. Case C: Two largest generators in Tabuk-2 are removed, remaining capacity 803.2 MW.
4. Case D: Three largest generators in Tabuk-2 are removed, remaining capacity 737.7 Mw.
5. Case E: Four largest generators in Tabuk-2 are removed, remaining capacity 673.2 Mw.

Table 5.2: Shows battery constraints.

Battery Constraints	
$\overline{P_B}$	50 MW
$\overline{E}$	250 MWh
$\underline{E}$	50 MWh
η_{in}, η_{out}	92 %

Table 5.3: shows the optimal operation cost for all the cases.

Case	**Scenario**	**PV**	**Best Integer Solution ($)**	**Time (S)**	**Gap**	**Penetration During the Day/Night**		
						Tabuk-1	**Tabuk-2**	**Battery**
A	1	ON	372,157.63	5.4	0.06%	No	Yes	Yes
	2	OFF	400,753.56	7.9	0.04%	No	Yes	Yes
B	1	ON	381,402.58	9.6	0.09%	No	Yes	Yes
	2	OFF	411,176.83	9.6	0.02%	No	Yes	Yes
C	1	ON	389,417.36	1.1	0.0003%	No	Yes	Yes
	2	OFF	426,429.99	3.6	0.0045%	Yes	Yes	Yes
D	1	ON	406,474.32	3.1	0.01%	No	Yes	Yes
	2	OFF	452,259.31	11.1	0.01%	Yes	Yes	Yes
E	1	ON	432,883.13	4.6	0.02%	Yes	Yes	Yes
	2	OFF	516,537.07	60	0.1%	Yes	Yes	Yes

Table 5.3 shows the optimal operation cost of one minute simulation for the different cases. These particular cases are used here to determine whether the PV and battery can help in meeting demand with minimum operation cost or if they are able to replace generation in Tabuk-1 since it is an old station (> 30 years old) with a high operating fuel cost. For the first scenario of each case, except for Case E, the optimal operation cost is achieved when the PV is included without any penetration from Tabuk-1. Case E required Tabuk-1 to operate with both PV and battery to help to meet the demand with minimum operation cost because of the lack of power when four generators are out-of-service. Hence, the PV with the battery storage can replace Tabuk-1. Without the PV, (as shown in Cases C, D and E) Tabuk-1 with the battery helped the system to meet the demand at optimal operation cost even in the most extreme case when four generators are out-of-service due to a long term outage or maintenance. Also, without the PV, the battery helped to meet the demand with minimum operational cost as presented in Table 5.3. Comparing Tables 4.3 and 5.3 for Cases C and D indicates that the optimal operation costs for both cases in Table 4.3 are $429,380 and $456,660$, respectively; these costs were reduced when the battery was involved in the optimization process to $426,429 and $452,259, respectively, as shown in the second scenario of Cases C and D in Table 5.3.

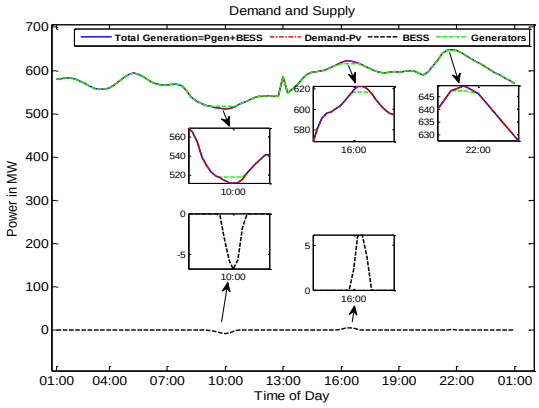

(a) Demand and supply.

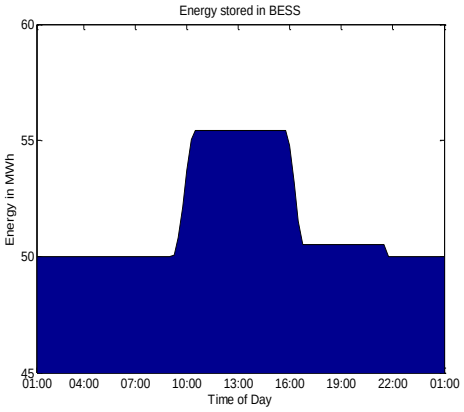

(b) BESS energy.

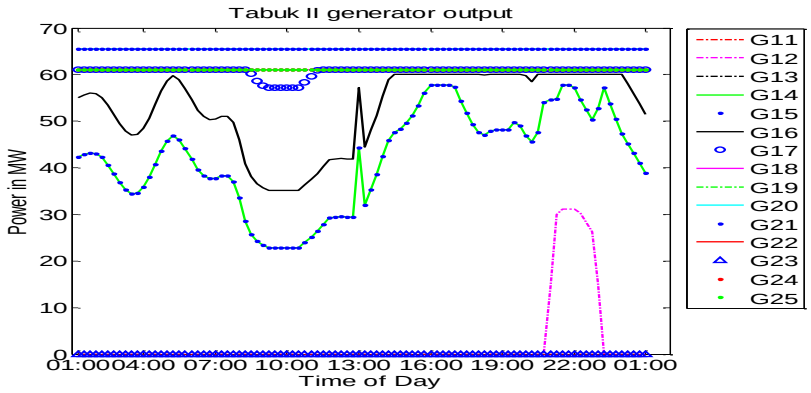

(c) Scheduled power for Tabuk-2.

Figure 5.3: Simulation result for case C scenario1.

In this study, three cases with results are selected. Figure 5.3 shows the simulation results for the first scenario of Case C when the two largest generators in Tabuk-2 were out-of-service for maintenance. As the results indicate, the energy stored in the battery operated within the battery energy limits. The power contribution of Tabuk-2 is presented in Figure 5.3(c); it was the only station with PV and BESS supplied the demand with optimal operation cost as shown in Table 5.3. As seen in the demand and supply graph in Figure 5.3(a), the battery began to charge approximately at 10 a.m. when extra power was available at minimum load, and then discharging at 4 p.m. and 10 p.m.

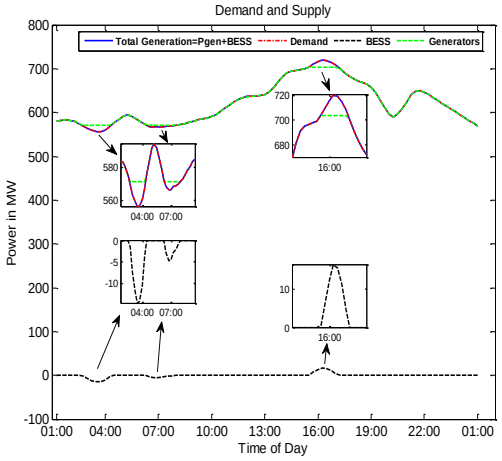

(a) Demand and supply.

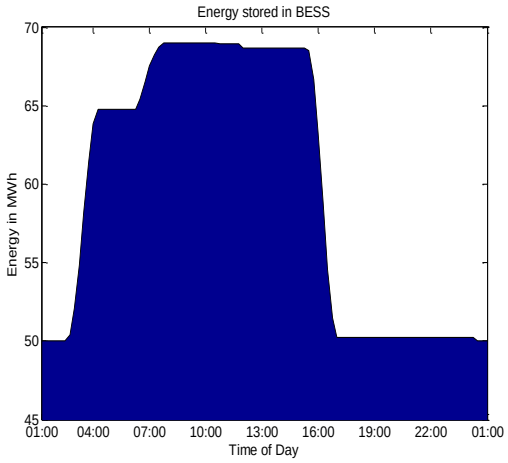

(b) BESS energy.

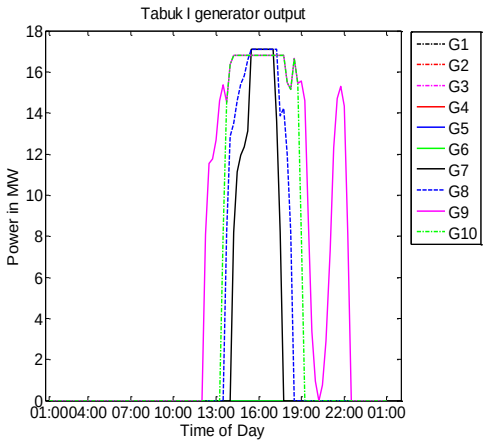

(c) Scheduled power for Tabuk-1.

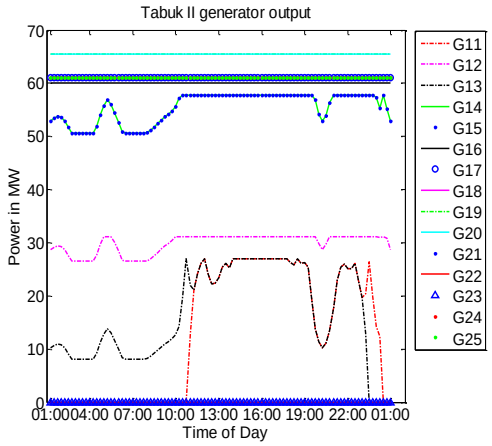

(d) Scheduled power for Tabuk-2.

Figure 5.4: Simulation result for case D scenario 2.

Figure 5.4 shows the simulation results for the second scenario in Case D. Since the PV and three largest generators in Tabuk-2 were not in operation, the battery helped to meet the demand at peak load by charging earlier in the day. Figure 5.4(a) shows the battery charged twice, once at approximately 4 a.m. and again at 7a.m. when there was extra power and then discharged later in the day at peak load, which occurred at 4 p.m., to support the

demand. The amount of power generated from each generator is shown in Figures 5.4(c) and (d).

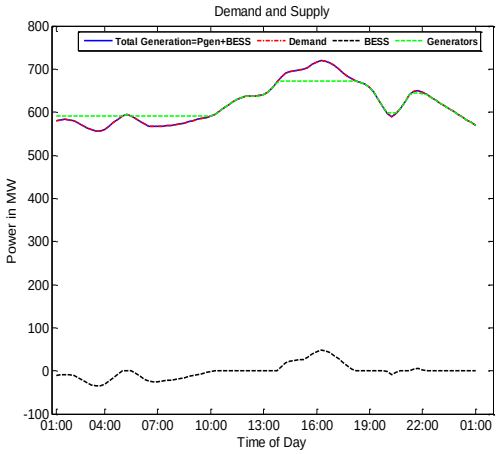

(a) Demand and supply.

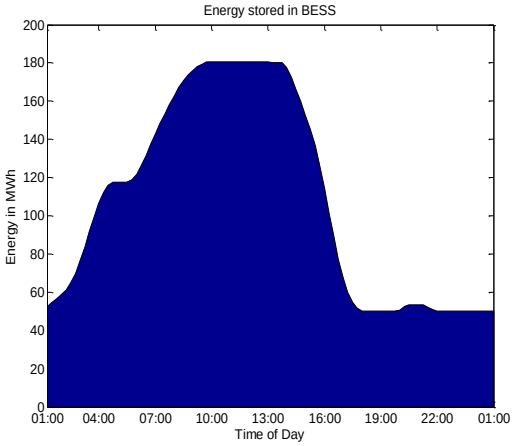

(b) BESS energy.

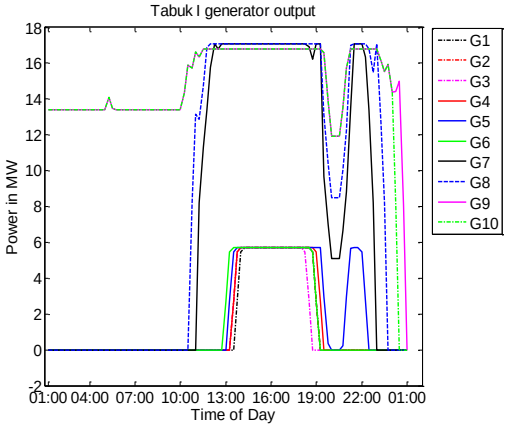

(c) Scheduled power for Tabuk-1.

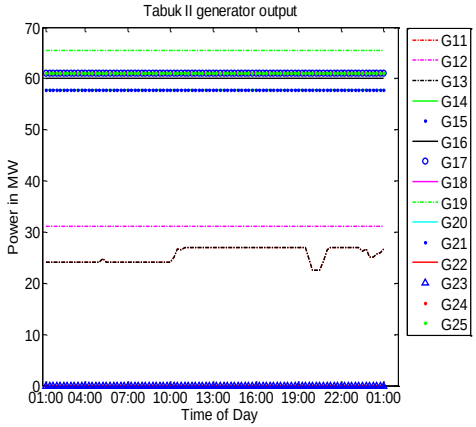

(d) Scheduled power for Tabuk-2.

Figure 5.5: Simulation result for case E scenario 2.

Figure 5.5 illustrates the results of the most extreme case when the PV and the four largest generators in Tabuk-2 were out-of-service for maintenance. As shown in Figure 5.5(a), the battery helped to meet demand by charging twice early in the morning for almost 8 hours in total. The lack of power during peak time was compensated by discharging the

battery from 2 p.m. to 6 p.m. when all generators were operating at full capacity of 673.2 MW. A second charging and discharging process occurred from approximately 8:30 p.m. to 10 p.m. respectively as shown in Figure 5.5(a).

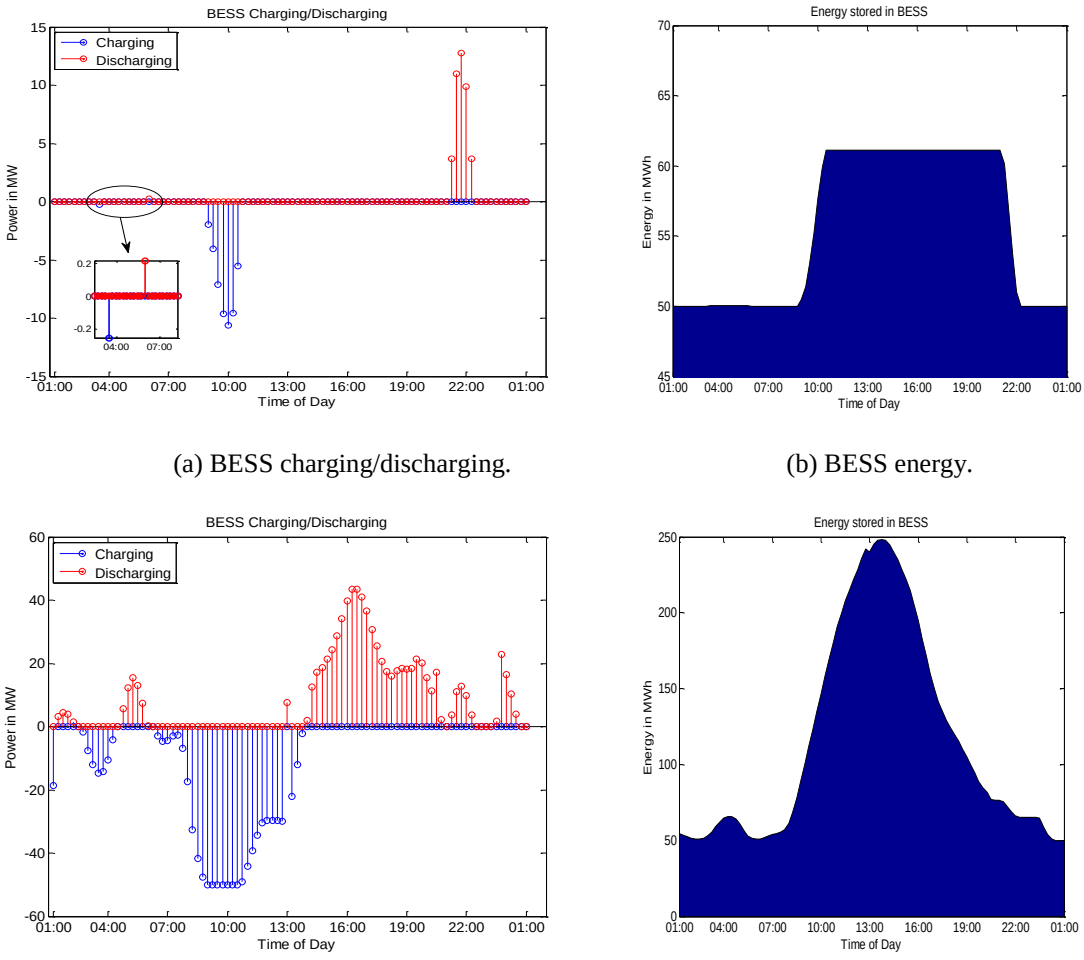

(a) BESS charging/discharging.

(b) BESS energy.

(c) BESS charging/discharging.

(d) BESS energy.

Figure 5.6: Simulation result for case B scenario1: (a) and (b) Battery usage cost included, (c) and (d) Battery usage cost excluded.

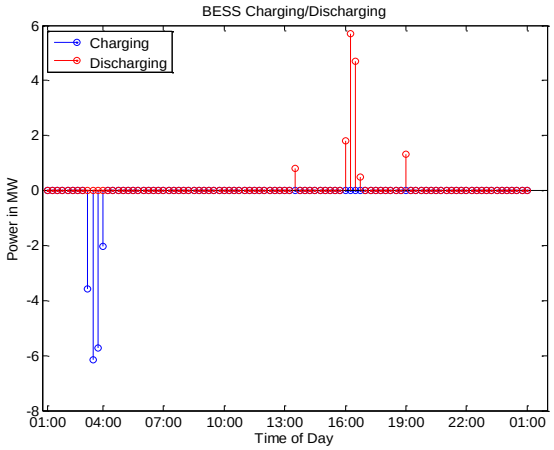

(a) BESS charging/discharging.

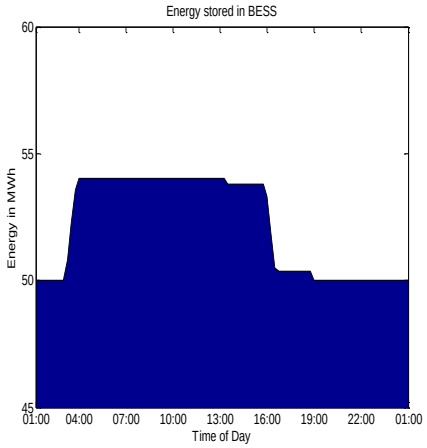

(b) BESS energy.

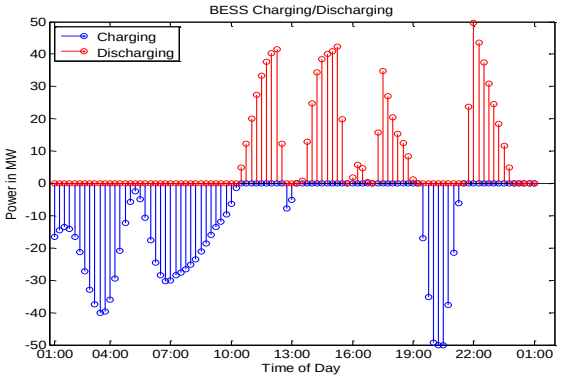

(c) BESS charging/discharging.

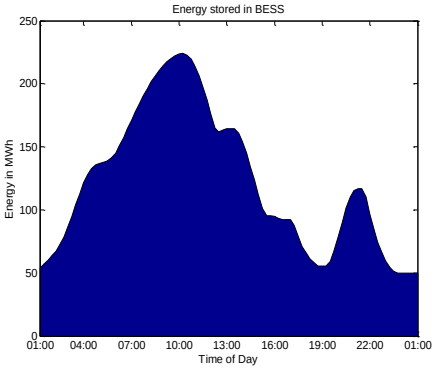

(d) BESS energy.

Figure 5.7: Simulation result for case A scenario 2: (a) and (b) Battery usage cost included, (c) and (d) Battery usage cost excluded.

Minimum operation cost and extended battery life have been achieved for all cases presented in Table 5.3. To determine the importance of including the battery life in the cost function, the usage cost of the battery is neglected. Figures 5.6 and 5.7 show the simulation results of two selected cases to illustrate the impact of the battery life both with and without the battery usage cost. The purpose of including the usage cost for the battery is to extend its life. In addition, the BESS has an associated life cycle that should be considered to

achieve optimal utilization of the battery. Charging/discharging the battery freely will impact the battery life cycle. Figures 5.6 and 5.7 show the impact of the battery life on the objective function. When the battery life is included, the BESS is utilized for two cycles while it is utilized for 4 cycles when the battery life is omitted as seen in Figures 5.6(a) and 5.6(c). In the cases seen in Figures 7(a)-(c), the number of cycles increased from 1 to 3 cycles when the battery usage cost was not considered. Table 5.4, which summaries the number of cycles utilized in each case, indicates a significant improvement to extend the battery life. In addition, more power is used for both charging and discharging process as more energy is stored since the battery is charging/discharging freely as shown in Figure 5.6(d) and Figure 5.7(d).

Table 5.4: Shows number of cycles performed for each case.

Case	**Scenario**	**No. of Cycle Utilized**	
		BESS life included	**BESS life excluded**
A	1	1	1
	2	1	3
B	1	2	4
	2	1	8
C	1	1	5
	2	1	4
D	1	1	6
	2	1	3
E	1	2	4
	2	2	4

Table 5.5: Optimal generated power at peak loads for each case with PV and battery.

Case	Scenario	Optimal Generated Power at Peak (MW)			
		Tabuk-2	Tabuk-1	PV	Battery
A	1	621.9523	0	98.0477	0
	2	714.3	0	0	5.7
B	1	621.9523	0	98.0477	0
	2	720	0	0	0
C	1	616	0	98.0477	5.9523
	2	701.2	16.8	0	2
D	1	621.9523	0	98.0477	0
	2	635.7	67.8	0	16.5
E	1	570.2	50.7	98.0477	1.0523
	2	570.2	102	0	47.8

Table 5.6: Observed violation cases.

Case	Scenario	Forced Contingency	Violated Line (%)	Solution
A	1	No violation occurred for all forced contingency		
	2	4-5	5-6 (112.1%)	6-4 or 6-9
		2-5	5-6 (101.3%)	1-4 or 4-8 or 6-4 or 6-9
B	1	No violation occurred for all forced contingency		
	2	4-5	5-6 (113.4%)	6-4 or 6-9
		2-5	5-6 (102.5%)	1-4 or 4-8 or 6-4 or 6-9
C	1	No violation occurred for all forced contingency		
	2	4-5	5-6 (110.5%)	6-4 or 6-9
D	1	No violation occurred for all forced contingency		
	2	No violation occurred for all forced contingency		
E	1	No violation occurred for all forced contingency		
	2	No violation occurred for all forced contingency		

In all cases, a violation is considered if a line achieves a 100% or more of its capacity. Table 5.5 shows the optimal generated power at peak loads for each case with the PV and battery penetration. Due to the size of the PV farm, it is not feasible to locate the PV farm within residential areas as it requires a large land area to accommodate it. Hence, the ideal location is near Bus 6 as presented in Chapter Two.

Table 5.6 shows only the cases of violations observed for any forced contingency as well as solution for relieving the overloaded lines. In these cases, the violations occurred only at line 5-6, which is mostly responsible for the delivery of power to Bus 9 which has the largest load. However, when the PV or Tabuk-1 is operating with the battery no violation occurred.

5.7 Summary

In this chapter, an MIQP based optimization problem was formulated in order to find the optimal operation schedule for generators in an isolated northwest grid of Saudi Arabia in the presence of renewable generation and battery storage. The BESS was embedded in the optimization problem by introducing a usage cost based on battery markets and prices for a large-scale storage. The results show substantial improvement both in the longevity of the BESS and in the economic and secure operation of the test system. This research also presented various cases to evaluate system reliability for any short term outages during optimal operation. Feasible solutions were provided for the violations investigated in order to maintain an optimal operation cost for a power system.

CHAPTER 6

Summary and General Conclusion

This chapter provides a summary of the dissertation objectives and its contributions. Also, it summaries the research work accomplished in each chapter with suggestions for future work.

A. Objectives of Dissertation

The dissertation objectives are as follows:

- Collect data and model the grid of the isolated northwest grid of Saudi Arabia in PSCAD for the research study.
- Model the PV and Battery control scheme.
- Investigate and solve the harmonic issue due to the PV penetration and the nonlinear loads.
- Achieve secure operation and optimal generation scheduling in presence of renewable energy.
- Etxended battery life has been achieved by introducing a usage cost for the battery that included in the objective function.
- Solution for all contingency is provided to have secure operation with optimal generation scheduling.

B. General Conclusion

While fossil fuels have traditionally been seen the primary sources of energy in the modern world, renewable option have been the subject of discussion for many years in the power industry. In addition to addressing the variability in fuel prices, they also offer a clean, low emission energy source, one that can improve the environment. One of the reliable natural sources of renewable energy integrates a PV system in the power grid, an approach that has experienced increasing use to environmental awareness and concerns about climate change.

The Kingdom of Saudi Arabia faces a high demand for energy due to its recent population growth and development in the industrial sectors. In the past ten years, between 2004 and 2014, the load demand has more than doubled, and it is expected to reach 120 GW by 2032. Moreover, the fuel consumption for energy, industry and transportation is expected to increase from 3.4 to 8.3 million barrels per day by 2028. The government is focused on taking appropriate actions to address this demand for energy and to reduce the Kingdom's reliance on fossil fuel since gas and oil exports constitute much of its revenue. The Kingdom's geographical location, vast land area, lack of rainfall, and year-round sunshine make it a good candidate a large-scale PV farm. One of the most promising locations for this farm is the northwest area of the country which has a high daily average of DNI rates.

Since it is the most promising, this study used the grid in this area for its investigation of the application of a PV system, including a complete simulation and analysis of the system. The grid data used were provided by the SEC, Tabuk branch, the grid and the PV

system control scheme with battery storage are modeled using PSCAD. As part of this study, the power system harmonics problem and its impact on power quality were investigated. This issue is an important consideration due to the continuous increase of grid connected PV and nonlinear loads since both introduce harmonics into the power system. Three types of nonlinear loads were included in this harmonic analysis, and the solution was to add a single tuned filter to eliminate the harmonic at the dominant harmonic frequency. The harmonics limits of each load then fell within the acceptable limits. In addition, the harmonic penetration from the PV side was also within the acceptable limits even when the nonlinear loads were included in the system as shown in Chapter Three.

Renewable energy systems today are sufficiently developed to be widely used to address environmental and economic dispatch (ED) concerns. However, the random power output of the PV rises many challenges in power system operation, with one solutions for addressing the challenge of solar variability being the use of battery storage. For this to be effective, optimal generation scheduling needs to consider battery life and short term outages so that the system can quickly responds to an outage without affecting the optimal operation. This study formulated an MIQP-based optimization to find the optimal operation schedule for the generators. Enhancing the battery life was accomplished by introducing a usage cost for the battery into the optimization problem based on battery prices and markets. In addition, the system reliability for any short term outages during optimal operation was evaluated by applying various cases to lead the system to achieve both secure and optimal operation.

C. Contribution of the dissertation

The contributions accomplished in this dissertation are as follows:

- Complete simulation and analysis of PV integration with storage interconnected to the northwest grid of Saudi Arabia [80].
- The power quality study includes nonlinear loads in addition of the PV penetration with storage [81].
- Optimal and secure operation has been achieved.

D. Future Work

The following suggestions can be completed after this dissertation:

- Transient analysis during switching operation in the presence of renewable resources.
- Study the impact of nonlinear loads and harmonic penetration on the protection devices.
- Investigate different types of faults when the battery acts as load (during charging process).

REFERENCES

[1] R. R. Obaid and A. H. Mufti, "Present state, challenges, and future of power generation in Saudi Arabia," in *Energy 2030 Conference*, 2008, pp. 1-6.

[2] "Report of activity (2002-2005)," Electricity & Cogeneration Regulatory Authority (ECRA)2005.

[3] "Annual Report " Saudi Electricity Company (SEC) 2014.

[4] "Annual Statistical Industries Booklet for Electricity and Seawater Desalination Industries," Electricity & Cogeneration Regulatory Authority (ECRA) 2014.

[5] (02/10/2015). *Electricity & Cogeneration Regulatory Authority (ECRA). Data and Satistics, Peak Load* Available:http://www.ecra.gov.sa/en.us/DataAndStatistics/NationalRecord/PeakLoad/pages/Home.aspx

[6] (10/29/2014). *King Abdullah City for Atomic and Renewable Energy (K.A.CARE). The Vision*. Available:https://www.kacare.gov.sa/en/FutureEnergy/Pages/vision.aspx

[7] S. AlYahya and M. A. Irfan, "New Solar Radiation Atlas for Saudi Arabia," in *International Conference on Renewable Energy Research and Application (ICRERA)*, 2014, pp. 245-249.

[8] S. Rehman, M. A. Bader, and S. A. Al-Moallem, "Cost of solar energy generated using PV panels," *Renewable and Sustainable Energy Reviews*, vol. 11, pp. 1843-1857, 2007.

[9] A. Hepbasli and Z. Alsuhaibani, "A key review on present status and future directions of solar energy studies and applications in Saudi Arabia," *Renewable and Sustainable Energy Reviews*, vol. 15, pp. 5021-5050, 2011.

[10] A. H. Almasoud and H. M. Gandayh, "Future of solar energy in Saudi Arabia," *Journal of King Saud University-Engineering Sciences*, vol. 27, pp. 153-157, 2015.

[11] (12/10/2014). *Deset Solar: Saudi Arabia Top 10 - Solar Projects Saudi Arabia*. Available: http://desertsolarsaudiarabia.com/top-10-solar-projects-ksa/

[12] E. Zell, S. Gasim, S. Wilcox, S. Katamoura, T. Stoffel, H. Shibli, *et al.*, "Assessment of solar radiation resources in Saudi Arabia," *Solar Energy*, vol. 119, pp. 422-438, 2015.

[13] S. H. Alawaji, "Evaluation of solar energy research and its applications in Saudi Arabia—20 years of experience," *Renewable and Sustainable Energy Reviews*, vol. 5, pp. 59-77, 2001.

[14] (11/25/2014). *The Saudi Arabia Solar Industry Association (SASIA). SolarGIS Data*. Available: http://saudi-sia.com/solargis-data/

[15] S. Rehman and I. El-Amin, "Performance evaluation of an off-grid photovoltaic system in Saudi Arabia," *Energy*, vol. 46, pp. 451-458, 2012.

[16] (11/25/2014). *Renewable Resource Atlas of Saudi Arabia*. Available: https://rratlas.kacare.gov.sa/RRMMPublicPortal/?q=en/News

[17] A. D. Rajapakse and D. Muthumuni, "Simulation tools for photovoltaic system grid integration studies," in *IEEE Electrical Power & Energy Conference (EPEC)*, 2009, pp. 1-5.

[18] Y. M. Tung, A. P. Hu, and N.-K. Nair, "Evaluation of micro controller based maximum power point tracking methods using dSPACE platform," in *Australian University Power Engineering Conference*, Auckland, 2006.

[19] Z. Yu and K. Ogboenyira, "Renewable Energy Through Micro-Inverters," *Power Electronics Technology*, vol. 1, Apr 2009.

[20] S. Jiang, "Battery Component in PSCAD/EMTDC," *Manitoba HVDC Research Centre, Winnipeg*, 2012.

[21] A. Yazdani and P. P. Dash, "A control methodology and characterization of dynamics for a photovoltaic (PV) system interfaced with a distribution network," *IEEE Transactions on Power Delivery*, vol. 24, pp. 1538-1551, 2009.

[22] F. Mahmood, L. Vanfretti, and H. Hooshyar, "Modeling of a detailed photovoltaic generation system for EMT-type simulation," in *Energy Conference (ENERGYCON),IEEE International*, 2014, pp. 916-921.

[23] O. Tremblay, L.-A. Dessaint, and A.-I. Dekkiche, "A generic battery model for the dynamic simulation of hybrid electric vehicles," in *IEEE Vehicle power and propulsion conference (VPPC)*, 2007, pp. 284-289.

[24] A. Clarke, H. Bihani, E. Makram, and K. Corzine, "Fault Analysis on an Unbalanced Distribution System in the Presence of Plug-In Hybrid Electric Vehicles," in *Clemson Power System Conference*, Clemson, 2013.

[25] T. Alquthami and R. R. Obaid, "An adaptive dynamic model of the western power grid of Saudi Arabia," in *Innovative Smart Grid Technologies-Middle East (ISGT Middle East), IEEE PES Conference*, 2011, pp. 1-6.

[26] (05/22/2013). *Electricity & Cogeneration Regulatory Authority (ECRA). Data and Satistics*. Available: http://www.ecra.gov.sa/en.us/dataandstatistics/pages/DataAndStatistics.aspx

[27] "Annual Repoert " Saudi Electricity Company (SEC)2013.

[28] A. A. Salam, "Population and Household Census, Kingdom of Saudi Arabia 2010: Facts and Figures," *International Journal of Humanities and Social Science*, vol. 3, 2013.

[29] R. N. Rao, "Harmonic Analysis of Small Scale Industrial Loads and Harmonic Mitigation Techniques in Industrial Distribution System," *International Journal of Engineering Research and Applications*, vol. 3, pp. 1511-1540, 2013.

[30] M. Fauri, "Harmonic modelling of non-linear load by means of crossed frequency admittance matrix," *IEEE transactions on Power systems*, vol. 12, pp. 1632-1638, 1997.

[31] U. P. BalaRaju, B. Kethineni, R. Shewale, and S. Grourishetti, "Harmonic Effects and Its Mitigation Techniques for a Nonlinear Load," *International Journal of Advanced Technology & Engineering Research*, vol. 2, pp. 122-127, 2012.

[32] B. Badrzadeh, K. S. Smith, and R. C. Wilson, "Designing passive harmonic filters for an aluminum smelting plant," *Industry Applications, IEEE Transactions on*, vol. 47, pp. 973-983, 2011.

[33] G. J. Wakileh, *Power systems harmonics: fundamentals, analysis and filter design*: Springer Science & Business Media, 2001.

[34] T. Gonen, *Electrical Power Distribution System Engineering*: CRC Press, New York, 2008.

[35] C. Sankaran, *Power quality*: CRC press, 2001.

[36] M. McGranaghan, "Overview of the guide for applying harmonic limits on power systems-IEEE P519A," in *Harmonics and Quality of Power Proceedings, 1998. Proceedings. 8th International Conference On*, 1998, pp. 462-469.

[37] C.-C. Kuo, "A novel coding scheme for practical economic dispatch by modified particle swarm approach," *IEEE Transactions on Power Systems*, vol. 23, pp. 1825-1835, 2008.

[38] B. H. Chowdhury and S. Rahman, "A review of recent advances in economic dispatch," *IEEE Transaction on Power System*, vol. 5, pp. 1248–1259, 1990.

[39] A. J. Wood and B. F. Wollenberg, *Power generation, operation, and control*: John Wiley & Sons, 2012.

[40] K. Lee, Y. Park, and J. Ortiz, "Fuel-cost minimisation for both real-and reactive-power dispatches," in *Generation, Transmission and Distribution, IEE Proceedings C*, 1984, pp. 85-93.

[41] Z.-X. Lian and J. D. Glover, "A zoom feature for a dynamic programming solution to economic dispatch including transmission losses," *IEEE Transactions on Power Systems*, vol. 7, pp. 544-550, 1992.

[42] V. Karthikeyan, S. Senthilkumar, and V. Vijayalakshmi, "A New Approach to the Solution of Economic Dispatch Using Particle Swarm Optimization with Simulated Annealing," *International Journal on Computational Sciences & Applications (IJCSA)*, vol. 3, pp. 37-49, 2013.

[43] F. Gherbi and F. Lakdja, "Environmentally constrained economic dispatch via quadratic programming," in *International Conference on Communications, Computing and Control Applications (CCCA)*, 2011, pp. 1-5.

[44] J. J. Grainger and W. D. Stevenson, *Power system analysis*: McGraw-Hill, 1994.

[45] J. Zhu, *Optimization of power system operation* vol. 47: John Wiley & Sons, 2015.

[46] N. D. Thitu, "Security Constrained Economic Dispatch Using Genetic Algorithm," Bs. Dissertation, Department of Electrical Engineering, University of Nairobi, Nairobi, 2014.

[47] R. Ouiddir, M. Rahli, and L. A.-. Koridak, "Economic Dispatch Using a genetic algorithm. Application to western Algeria's Electrical power Network," *Journal of Information Science and Engineering,* vol. 21, pp. 665-668, 2005.

[48] S. DUMAN, A. ÖZTÜRK, M. K. DÖŞOĞLU, and S. TOSUN, "Economic Dispatch by Using Different Crossover Operators of Genetic Algorithm," *Journal of Eelectrical & Electronics Engineering,* vol. 10, pp. 1173-1183, 2010.

[49] G. K. Babu and R. K. Samala, "Network and Generator Constrained Economic Dispatch Using Real and Binary Coded Genetic Algorithms," *G Kalidas Babu et al Int. Journal of Engineering Research and Applications,* vol. 3, pp. 1185-1192, 2013.

[50] D. Axehill, "Integer quadratic programming for control and communication," Ph.D Dissertation, Depaetment of Electrical Engineering, , Linkoping University, Sweden, 2008.

[51] A. Bemporad and M. Morari, "Control of systems integrating logic, dynamics, and constraints," *Automatica,* vol. 35, pp. 407-427, 1999.

[52] (25/02/2016). *Mixed Integer Quadratic Program (MIQP), Free Matlab Toolbox for optimization*. Available:http://www.i2c2.aut.ac.nz/Wiki/OPTI/index.php/Probs/MIQP.

[53] C. A. Floudas, *Nonlinear and mixed-integer optimization: fundamentals and applications*: Oxford University Press on Demand, 1995.

[54] L. A. Wolsey, *Integer programming* vol. 42: Wiley New York, 1998.

[55] (2016). *The ILOG CPLEX*. Available: https://www.ibm.com/developerworks/downloads /ws/ilogcplex/

[56] M. Carrión and J. M. Arroyo, "A computationally efficient mixed-integer linear formulation for the thermal unit commitment problem," *EEE Transactions on Power Systems,* vol. 21, pp. 1371-1378, 2006.

[57] G. Morales-España, J. M. Latorre, and A. Ramos, "Tight and compact MILP formulation for the thermal unit commitment problem," *EEE Transactions on Power Systems,* vol. 28, pp. 4897-4908, 2013.

[58] (2014, 01/5/2014). *Electricity & Cogeneration Regulatory Authority (ECRA), Generation Capacity*. Available: http://www.ecra.gov.sa/ar-sa/dataandstatistics

[59] Y. Oka and A. Yokoyama, "Optimal operation scheduling and economical evaluation method of battery energy storage system in power system with a large penetration of photovoltaic generation," in *IEEE PowerTech (POWERTECH)*, Grenoble, 2013, pp. 1-6.

[60] M. Marwali, M. Haili, S. Shahidehpour, and K. Abdul-Rahman, "Short term generation scheduling in photovoltaic-utility grid with battery storage," *IEEE Transactions on Power Systems,* vol. 13, pp. 1057-1062, 1998.

[61] B. H. Chowdhury and S. Rahman, "Analysis of interrelationships between photovoltaic power and battery storage for electric utility load management," *IEEE Transactions on Power Systems,* vol. 3, pp. 900-907, 1988.

[62] R. Fischl, P. Herczfeld, T. Halprin, and D. Stewart, "Design of integrated-electric-solar-utility system for peak load shaving," in *Proceedings of the IEEE Power Engineering Soc. Winter Meeting, New York, paper A*, 1979, pp. 102-105.

[63] F. Pazheri, N. Malik, and O. Safoora, "Economic and environmental dispatch at high potential solar area with renewable storage," *International Journal of Environmental Science and Development* vol. 3, pp. 177-182, 2012.

[64] G. Haddadian, N. Khalili, M. Khodayar, and M. Shahidehpour, "Optimal scheduling of distributed battery storage for enhancing the security and the economics of electric power systems with emission constraints," *Electric Power Systems Research,* vol. 124, pp. 152-159, 2015.

[65] Y. Levron and D. Shmilovitz, "Power systems' optimal peak-shaving applying secondary storage," *Electric Power Systems Research,* vol. 89, pp. 80-84, 2012.

[66] J.-H. Teng, S.-W. Luan, D.-J. Lee, and Y.-Q. Huang, "Optimal charging/discharging scheduling of battery storage systems for distribution systems interconnected with sizeable PV generation systems," *IEEE Transactions on Power Systems*, vol. 28, pp. 1425-1433, 2013.

[67] Z. Ziadi, S. Taira, M. Oshiro, and T. Funabashi, "Optimal power scheduling for smart grids considering controllable loads and high penetration of photovoltaic generation," *IEEE Transactions on Smart Grid*, vol. 5, pp. 2350-2359, 2014.

[68] Y. Riffonneau, S. Bacha, F. Barruel, and S. Ploix, "Optimal power flow management for grid connected PV systems with batteries," *IEEE Transactions on Sustainable Energy*, vol. 2, pp. 309-320, 2011.

[69] S. Nuchprayoon, "Optimum scheduling of non-utility facility with battery storage under a price-taking scheme," in *IEEE PowerTech*, Eindhoven 2015, pp. 1-6.

[70] (2015, 08/31/2015). *Renewable Resource Atlas of Saudi Arabia*. Available: https://rratlas.kacare.gov.sa

[71] M. Lave and J. Kleissl, "Testing a wavelet-based variability model (WVM) for solar PV power plants," in *IEEE Power and Energy Society General Meeting*, 2012, pp. 1-6.

[72] M. Lave, J. Kleissl, and J. S. Stein, "A wavelet-based variability model (WVM) for solar PV power plants," *IEEE Transactions on Sustainable Energy*, vol. 4, pp. 501-509, 2013.

[73] (2016, 02/25/2016). *Levelived cost of energy storage, Renew economy*. Available: http://reneweconomy.com.au/2015

[74] A. A. Akhil, G. Huff, A. B. Currier, B. C. Kaun, D. M. Rastler, S. B. Chen, *et al.*, *DOE/EPRI 2013 electricity storage handbook in collaboration with NRECA*: Sandia National Laboratories Albuquerque, NM, USA, 2013.

[75] L. T and S. D, "Short term generation scheduling of a microgrid," in *2009 IEEE (TENCON) Region 10 Conf*, Singapore, 2009, pp. 1-6.

[76] W. Ongsakul and N. Petcharaks, "Unit commitment by enhanced adaptive Lagrangian relaxation," *IEEE Transactions on Power Systems,* vol. 19, pp. 620-628, 2004.

[77] Z. Ouyang and S. Shahidehpour, "An intelligent dynamic programming for unit commitment application," *IEEE Transactions on Power Systems,* vol. 6, pp. 1203-1209, 1991.

[78] N. P. Padhy, "Unit commitment-a bibliographical survey," *IEEE Transactions on Power Systems,* vol. 19, pp. 1196-1205, 2004.

[79] K. Baker, G. Hug, and X. Li, "Optimal storage sizing using two-stage stochastic optimization for intra-hourly dispatch," in *North American Power Symposium (NAPS)*, 2014, pp. 1-6.

[80] H. Albalawi, E. Makram, and T. Alogla, "PV penetration with battery storage for an isolated northwest Grid of Saudi Arabia," in *North American Power Symposium (NAPS)*, 2015, pp. 1-6.

[81] H. Albalawi and E. Makram, "Power Quality Study of an Isolated Northwest Grid of Saudi Arabia with PV and Storage," *Journal of Power and Energy Engineering,* vol. 3, pp. 54-64, 2015.

APPENDICES

APPENDIX A: Line and Load data.

Table A. 1: Line and Peak load data.

From Bus	To Bus	R (Ohm/Km)	X (Ohm/Km)	Capacity MVA	Bus No.	Peak Load (MW)
1	2	0.0493	0.2408	294.2	1	106
1	4	0.0493	0.2408	294.2	2	94
2	3	0.047	0.25	294.2	3	55
2	5	0.0773	0.4682	289.1	4	62
2	7	0.08606	0.5062	322.7	5	11
3	10	0.0493	0.2408	294.2	6	37
4	5	0.0773	0.4682	289.1	7	60
4	6	0.093	0.452	322.7	8	67
4	8	0.0493	0.2408	294.2	9	134
4	9	0.047	0.25	294.2	10	12
5	6	0.094	0.458	322.7	11	33
5	7	0.0794	0.4671	322.7	12	43
6	9	0.0493	0.2408	294.2	Total	720
10	8	0.0493	0.2408	294.2		
5 (2)	12 (2)	0.08	0.47	358.3		
6 (2)	11 (2)	0.149	0.497	358.3		

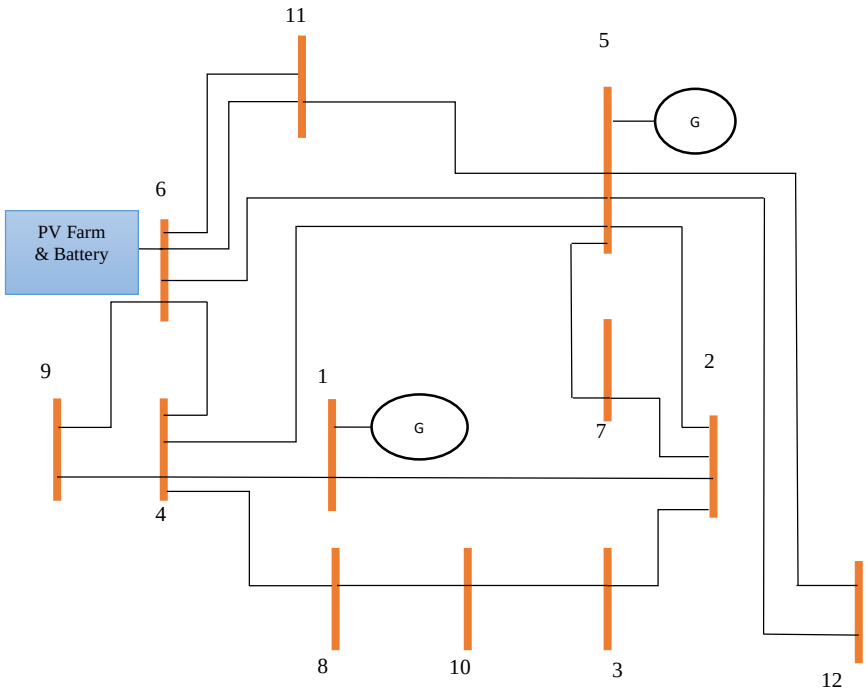

Figure A. 1: Single line diagram of Tabuk grid.

APPENDIX B: Nomenclature

Binary Variables

β_i	Variable to enforce fixed cost of i^{th} generator.
γ_i	Variable to enforce startup cost of i^{th} generator.

Continuous Variables

$\Delta P_i^g(t)$	Rate of change of power output of i^{th} generator in period t.
$E(t)$	Energy stored in period t.
$P_i^g(t)$	Power output of i^{th} generator in period t.
$P_{pv}(t)$	PV Power output in period t.
$P^C(t), P^D(t)$	Rate of charge and discharge Power in period t.
$P_{LD}(t)$	Load demand in period t.

Parameters

a_i, b_i, c_i	Fuel cost coefficients of i^{th} generator.
$nGen$	Number of generators.
$\overline{P_i^g}$	Upper limit of real power generation of i^{th} generator.
$\underline{P_i^g}$	Lower limit of real power generation of i^{th} generator.
$\overline{\Delta P_i^g}$	Maximum ramp up rate of i^{th} generator.

$\underline{\Delta P_i^g}$	Minimum ramp down rate of i^{th} generator.
$\overline{E}$	Maximum Energy rating of battery storage.
$\underline{E}$	Minimum Energy rating of battery storage.
$\overline{P_B}$	Power rating of energy storage.
η_{in}, η_{out}	Battery storage charge and discharge efficiency.
$C_{i,str}^g$	Startup cost of i^{th} generator.
C_B	Usage cost of the Battery.
Δt	Dispatch interval.
T	Set of all dispatches included in optimization horizon.